NASA/TM– 20250004188

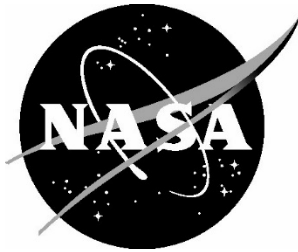

Modeling Data Acquisition System Measurement Uncertainty Using the Monte Carlo Method

Francisco Peña and Erick Rossi De La Fuente
Armstrong Flight Research Center, Edwards, California

April 2025

NASA STI Program Report Series

Since its founding, NASA has been dedicated to the advancement of aeronautics and space science. The NASA scientific and technical information (STI) program plays a key part in helping NASA maintain this important role.

The NASA STI program operates under the auspices of the Agency Chief Information Officer. It collects, organizes, provides for archiving, and disseminates NASA's STI. The NASA STI program provides access to the NTRS Registered and its public interface, the NASA Technical Reports Server, thus providing one of the largest collections of aeronautical and space science STI in the world. Results are published in both non-NASA channels and by NASA in the NASA STI Report Series, which includes the following report types:

- TECHNICAL PUBLICATION. Reports of completed research or a major significant phase of research that present the results of NASA Programs and include extensive data or theoretical analysis. Includes compilations of significant scientific and technical data and information deemed to be of continuing reference value. NASA counterpart of peer-reviewed formal professional papers but has less stringent limitations on manuscript length and extent of graphic presentations.
- TECHNICAL MEMORANDUM. Scientific and technical findings that are preliminary or of specialized interest, e.g., quick release reports, working papers, and bibliographies that contain minimal annotation. Does not contain extensive analysis.
- CONTRACTOR REPORT. Scientific and technical findings by NASA-sponsored contractors and grantees.
- CONFERENCE PUBLICATION. Collected papers from scientific and technical conferences, symposia, seminars, or other meetings sponsored or co-sponsored by NASA.
- SPECIAL PUBLICATION. Scientific, technical, or historical information from NASA programs, projects, and missions, often concerned with subjects having substantial public interest.
- TECHNICAL TRANSLATION. English-language translations of foreign scientific and technical material pertinent to NASA's mission.

Specialized services also include organizing and publishing research results, distributing specialized research announcements and feeds, providing information desk and personal search support, and enabling data exchange services.

For more information about the NASA STI program, see the following:

- Access the NASA STI program home page at http://www.sti.nasa.gov

.

NASA/TM– 20250004188

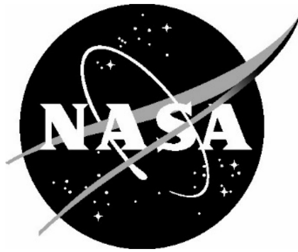

Modeling Data Acquisition System Measurement Uncertainty Using the Monte Carlo Method

Francisco Peña and Erick Rossi De La Fuente
Armstrong Flight Research Center, Edwards, California

National Aeronautics and
Space Administration

Armstrong Flight Research Center
Edwards, California 93523

April 2025

The use of trademarks or names of manufacturers in this report is for accurate reporting and does not constitute an official endorsement, either expressed or implied, of such products or manufacturers by the National Aeronautics and Space Administration.

Available from:

NASA STI Program / Mail Stop 050
NASA Langley Research Center
Hampton, VA 23681-2199

Abstract

In support of furthering structural research in the National Aeronautics and Space Administration Armstrong Flight Research Center (Edwards, California) Flight Loads Lab, a measurement uncertainty study is being conducted of the primary analog data acquisition systems. The Flight Loads Lab performs several structural tests on a yearly basis, including mechanical and thermal testing of aerospace components or flight vehicles, to calibrate and evaluate flight loads instrumentation under the conditions expected in flight. During ground testing, analog sensors are used to collect vital data about the structural performance of test articles. These analog sensors include strain gages, thermocouples, load cells, string potentiometers, and linear variable differential transformers with demodulators. This report covers the process of using the Monte Carlo method applied to a data acquisition system and analog circuits for various sensors to obtain an estimate of uncertainty of the resulting measurements.

Nomenclature

AFRC	Armstrong Flight Research Center
b_k	k-th elemental systematic standard uncertainty
BCM	bridge completion module
C_ℓ	lead-wire resistance coefficient
DAS	data acquisition system
DRE	data reduction equation
DVM	digital voltmeter
DVM(…)	digital voltmeter function in the Monte Carlo script
$f[...]$	A function that represents the Data Reduction Equation
FB-T-I	Full-bridge, Type-I
FB-T-II	Full-bridge, Type-II
FB-T-III	Full-bridge, Type-III
FLL	Flight Loads Laboratory
G	amplifier gain
GF	gage factor
G_{prog}	Programmable amplifier gain
HB-T-I	Half-bridge, Type-I
HB-T-II	Half-bridge, Type-II
i	index indicating the iteration in the Monte Carlo simulation
J	electrical junction
L	length, in
LVDT	linear variable differential transformer
M	bending moment, in-lb
MCM	Monte Carlo method
N	number of iterations in the Monte Carlo method
NASA	National Aeronautics and Space Administration
p	potentiometer
P	axial load, lbf
randn	random number generator with normal distribution
R	resistor, ohm
Rg	strain-gage resistance
Ri	the target resistance in a Wheatstone bridge
R_ℓ	lead-wire resistance
RTD	resistance temperature detector

RTI	Referred to Input
RTO	Referred to Output
s_j	random standard uncertainty for the j-th measurand
SlidePos	voltage divider slide position
T	temperature
T_{true}	the true temperature
TC	thermocouple
Tj	temperature at the junction
T_{ref}	temperature of the reference block
u_ε	the sample standard deviation of the uncertainties in strain
u_j	sample standard deviation of the distribution of measurand *j*
U	measurement uncertainty
U_ε	measurement uncertainty in strain
U_j	expanded uncertainty of measurand *j*
ν	Poisson ratio
V_{ex}	circuit excitation voltage, volt
V_{in}	target input voltage to circuit, volt
V_{meas}	measured voltage, volt
V_{out}	circuit voltage output, volt
V_r	voltage difference ratio
V_{ref}	Voltage reference
V_{source}	function to generate excitation voltage
V_{true}	the true voltage
$\bar{x}$	mean
μ	micro (10^{-6})
γ	component of uncertainty due to random error
γ_j	component of uncertainty in j due to random error
γ_T	component of uncertainty in T, temperature, due to random error
γ_V	component of uncertainty in V, voltage, due to random error
α	thermocouple sensitivity slope, volt/°C
β	elemental systematic error
βk	k-th component of elemental systematic error
Δ	difference
ΔR	difference in resistance
ΔR_G	difference in resistance of gage
ΔT	difference in temperature
ε	axial strain, in/in
ϵ	strain gauge measured strain
Ω	ohm
σ	standard deviation
ν	Poisson ratio

Subscripts

1, 2, 3, 4	identifiers for multiple variables of the same type
G, g	gage resistor
ℓ	lead wire
displaced	displaced state
ref	reference state
strained	strained state
unstrained	unstrained state
true	the true value of a variable

j	any given measurand such as temperature, voltage, et cetera
k	any given source of elemental systematic standard uncertainty

1 Introduction

The Flight Loads Lab (FLL), which is part of the National Aeronautics and Space Administration (NASA) Armstrong Flight Research Center (AFRC) (Edwards, California), was constructed in 1964 to perform structural ground tests of aerospace components or full flight vehicles. Structural testing in the FLL includes combined (or isolated) mechanical and thermal load testing. These ground tests are carried out to evaluate vehicle concepts, design margins, and to calibrate flight instrumentation under the conditions expected in flight. To perform these complex structural tests, a data acquisition system (DAS) is used to obtain data from several hundred to several thousand sensor channels. The FLL DAS monitors several types of analog sensors that include, but are not limited to, strain gages, thermocouples, load cells, string potentiometers, and linear variable differential transformers (LVDTs) with demodulators.

This report provides a structured framework to estimate the measurement uncertainty of various analog sensors that are used for ground testing aerospace structures in the FLL. Often, customers would like to understand and quantify the uncertainty in measurement for each type of instrumentation used during testing in the FLL. The primary function of this report is to provide the theoretical and mathematical foundation needed to understand how the FLL estimates the measurement uncertainty for the instrumentation used with the DAS; the secondary function is to act as a guide for any engineer embarking on a similar endeavor while working in a laboratory setting. The Monte Carlo method was used to obtain an estimate of the measurement uncertainty using specifications from a representative data acquisition module and circuit equations for various analog sensors. Results of the Monte Carlo simulation are estimates of the contributions of the DAS to the overall uncertainty of the measurement.

2 The Monte Carlo Method

Multiple methods exist to estimate the measurement uncertainty of a physical quantity (or "measurand"). The measurand is often transformed into an electrical signal (usually a voltage) by a transducer (sometimes referred to as a sensor) which is then, typically, converted to a digital signal for storage; therefore, often the measurand is not measured directly, but is instead, calculated from voltage measurements which are input into a data reduction equation (DRE). For example, if an engineer would like to measure strain, a foil strain gage is placed on a test article that produces a voltage change caused by a wire-resistance change as the test article is stressed and deformed, which is directly measured by a voltmeter. Next, a DRE is used to calculate the measurand - strain in this case - using the voltage change, among other input variables such as temperature, gage factor, et cetera, through a known mathematical relationship. There are uncertainties, however, in the input variables used in the DRE which propagate through the equations to produce an uncertainty in the measurand. What remains unanswered is: how does one estimate the uncertainty in the measurand, calculated from the DRE, when there are various input variables each with associated uncertainties in their values?

One option to solve this problem is to use the Taylor series method for propagation of uncertainties when there are a small number of relatively simple analytical equations that represent the system. One only needs to calculate the partial derivatives of the DRE to estimate the uncertainty; however, when there are many complex and sometimes nonanalytical relationships used to describe the system, the result is a laborious and possibly erroneous calculation of the partial derivatives of the DRE (ref. 1). Alternatively, one could take advantage of the computational simplicity of the Monte Carlo method for the propagation of uncertainties within the DRE.

For this uncertainty analysis, the Monte Carlo method (MCM) was chosen to simulate measurement uncertainty of a representative data acquisition module used in the FLL. The Monte Carlo method is a commonly used method for propagating uncertainties throughout a system of equations; therefore, lending itself nicely to the complex DRE used to model the FLL DAS (refs. 1, 2, and 3).

The computational process of the MCM is depicted in figure 1. A set of input values to the DRE are assumed, and they represent the true values of these physical quantities. The goal is to determine the measurement uncertainty for a given set of input values; however, each input value will have random error γ and systematic error β associated with the measurement equipment. Each type of error has an associated error distribution function and associated standard deviation (denoted as a_j and b_k) for the random error distribution function and the systematic error distribution function, respectively.

To simulate a measurement, a random number generator is used to simulate each component of error by randomly choosing a component of error from its corresponding error distribution function, where in figure 1, γ_j and β_k correspond to any given component of random error or systematic error, respectively. To calculate the measurand, all the random and systematic errors are added to the true value of the measured input variable, and the input variables are plugged into the DRE (represented by the function f). This simulation of taking a measurement represents one of the N iterations that is necessary to characterize the distributions of measurements, in this case, strain ε, for example, thus, the simulation of measurement is repeated N times and results in a distribution of calculated measurand values from the DRE. The standard deviation u_ε of this distribution can be used to calculate the estimate of the expanded uncertainty U_ε for a given level of confidence. Typically, a 95-percent level of confidence is assumed in which case U_ε is equal to two times u_ε, colloquially referred to as two-sigma.

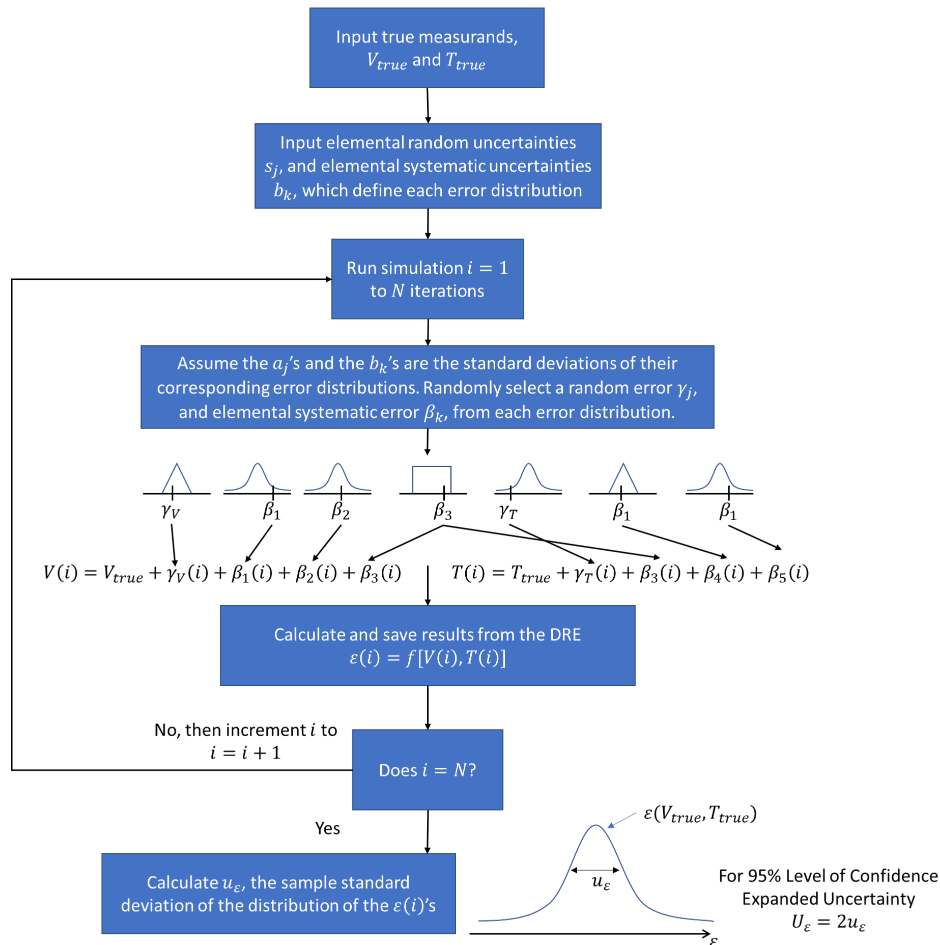

Figure 1. The Monte Carlo method algorithm used to estimate the expanded uncertainty, adapted from Coleman and Steele (ref. 1).

3 Modeling the Data Acquisition Modules

A typical DAS contains multiple subsystems to obtain a measurement. For the FLL DAS, subsystem models were developed for the following: 1) excitation voltage (V_{ex}); 2) amplifier/digitizer for the digital voltmeters (DVMs); and 3) bridge completion module (BCM), with bridge completion resistors (R1, R2, and R3). Figure 2 shows the conceptual layout of the DAS and test article. Specifications for the DAS subsystem models were obtained by using a specification sheet for the DAS modules used in the FLL. A list of the uncertainties used to model these subsystems are shown in table 1. This process can be adapted to represent any other data acquisition modules, assuming documentation regarding hardware performance is provided.

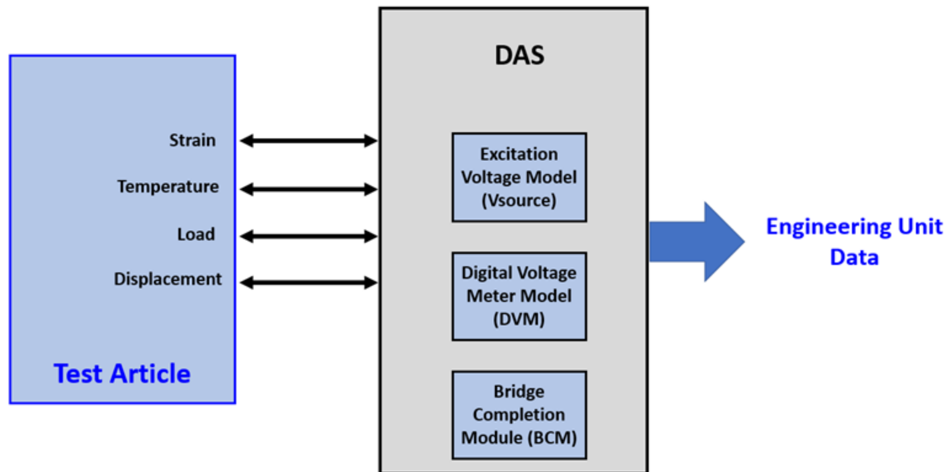

Figure 2. The conceptual layout of the data acquisition system and test article.

Figure 3 shows all reported uncertainties in the DAS specification sheets that are assumed to be a normal distribution, and specified uncertainty limits are assumed to define a 95-percent level of confidence within a normal distribution (e.g., ±2 standard deviations or ±2σ), with the mean value being the "true" value. A normal distribution random number generator ("randn") was used in the Monte Carlo simulation.

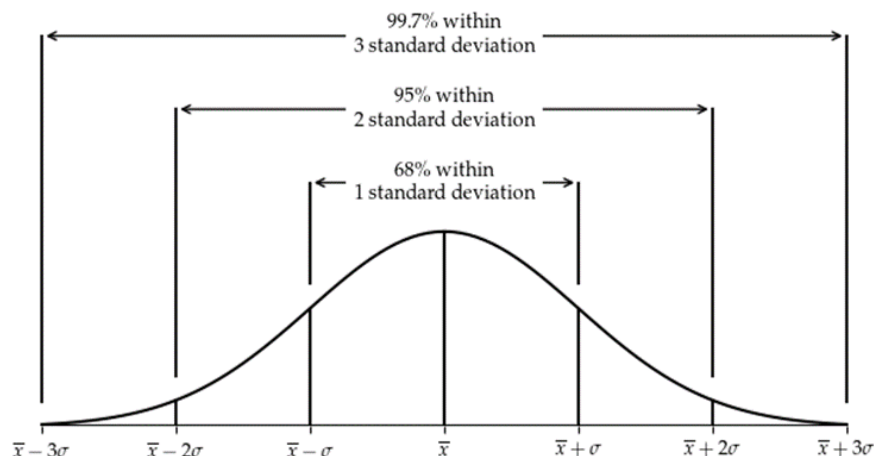

Figure 3. Normal distribution example.

Table 1 provides a list of uncertainties that are included in the Monte Carlo method; the list was obtained from a specification sheet of a representative data acquisition system module used in the Flight Loads Lab.

Table 1. List of uncertainties used in the Monte Carlo method.

	Excitation/Transducer Power	
D	Amount of Uncertainty	Description
U00	±0.1%	Target input voltage uncertainty
U01	±0.2%	Accuracy
U02	±0.01%	Stability
U03	±0.005%/°C	Temperature stability
U04	±200 μV	Excitation noise
	Amplifier	
ID	Amount of Uncertainty	Description
U05	±0.05%	Accuracy
U06	±0.01%	Gain stability
U07	±0.004%/°C	Gain temperature stability
U08	±0.01% for gain < 1,000 ±0.02% for gain > 1,000	Gain linearity
U09	±1.0 μV	Zero (amplifier) RTI
U10	±5.0 μV	Zero stability RTI
U11	±1.0 μV/°C	Zero temperature stability RTI
U12	±1.5 μV	Noise (1 kHz) RTI
U13	±0.5 mV	Zero (amplifier) RTO
U14	±1.0 mV	Zero stability RTO
U15	±0.2 mV/°C	Zero temperature stability RTO
	Filter	
ID	Amount of uncertainty	Description
U16	±2.0 mV	Noise (1 kHz) RTO
	Digitizer	
ID	Amount of uncertainty	Description
U17	±0.005%	Sample (droop) RTO
U18	±4 bits (2 LSB)	Digitizer linearity
	Bridge Completion Resistors	
ID	Amount of uncertainty	Description
U19	±0.01%	Accuracy
U20	±0.00031%/°C	Temperature stability

3.1 Voltage Excitation Source

Depending on the type of sensor, the sensing circuit may require an excitation voltage source. The FLL DAS is capable of providing source voltage to a sensor circuit (termed excitation voltage) and is programmable for each module from 0 to 12 volts. The excitation uncertainties (U00 to U04) from the

DAS module were included in the Monte Carlo simulation, previously shown in table 1. Within the simulation, a V_{source} function outputs the excitation voltage (V_{ex}) based on the programmable user input voltage (V_{in}) and the change in the ambient temperature (ΔT). The excitation voltage is recursively updated for each additional uncertainty component. A simplified example of pseudocode for the modeling of the voltage excitation source is shown in figure 4.

```
## Example pseudo-code, Model of programmable excitation voltage
# Model the excitation voltage produced by the DAS to energize sensor circuits.
# Use a random number generator with normal distribution (randn).
# The randn function has two inputs, the mean and the standard deviation
# randn(mean, standard deviation)
# Uncertainties are obtained from example data acquisition module
# specification sheets. See Table 1
# Inputs:
# Vin, user programmable excitation voltage
# del_Temp_C, change in ambient temperature
# Output:
# Vex = actual excitation voltage

def V_Source (Vin, del_Temp_C):

      # Sequentially including uncertainties (U00, U01, U02, U03 and U04) using a
      # random number generator with a normal distribution
      Vex = Vin
      Vex = Vex * randn(1.0, 0.1/100/2)
      Vex = Vex * randn(1.0, 0.2/100/2)
      Vex = Vex * randn(1.0, 0.01/100/2)
      Vex = Vex * randn(1.0, 0.005/100/2 * del_Temp_C)
      Vex = Vex + randn(0, 200e-6/2)

      return Vex
```

Figure 4. Simplified pseudocode for the modeling of the voltage excitation source.

3.2 Digital Voltmeter

The DAS amplifier, filter, sample and hold, and digitizer were modeled as an integrated unit and referred to as the digital voltmeter (DVM). The DVM is used to simulate how well the data acquisition system measures sensor output voltages, often referred to as V_{out}. The DVM model (termed DVM( ) function) is based on the uncertainties (U05 to U18) from the DAS module, as previously shown in table 1. Uncertainty included before amplification is called Referred to Input (RTI); uncertainties included after amplification is called Referred to Output (RTO). The digitizer can measure voltage in a range of ±10 volts, with a 16-bit resolution.

Depending on the desired measurement range, voltage going into the DVM (V_{out}) is amplified by a gain (G). Gain is user programmable (G_{prog}), but the actual gain used in the internal circuitry has uncertainties. Within the DVM model, measured voltage (V_{meas}) and gain are recursively updated for each additional uncertainty component. A simplified example of pseudocode for the modeling of the DVM function is shown in figure 5.

```
# Example pseudo-code, Digital Voltmeter(DVM) modeling
# Estimate the measured voltage by the DVM including all known
# uncertainties
# Use a random number generator with normal distribution (randn).
# The randn function has two inputs, the mean and the standard deviation
# randn(mean, standard deviation)
# Uncertainties are obtained from example data acquisition module
# specification sheets. See Table 1
# Inputs:
# Gprog, user programmed gain setting
# Vout, voltage output of sensor circuit, which is passed to the DVM
# del_Temp_C, ambient temperature
# Output:
# Vmeas = voltage measurement
def DVM(Vout, Gprog, del_Temp_C):
     # Estimate gain (G, given the programmable input Gprog)
     # Apply uncertainties (U05, U06, U07, U08) to G based on a normal distribution
     G = Gprog
     G = G * randn(1.0, 0.05/100/2)
     G = G * randn(1.0, 0.01/100/2)
     G = G * randn(1.0, del_Temp_C * 0.004/100/2)
     if G < 1000:
            gain_linearity = 0.01/100/2
     else:
            gain_linearity = 0.02/100/2
     G = G * randn(1.0, gain_linearity)
     # Add pre-amplified uncertainties, or Referred to Input (RTI) uncertainties
     # (U09, U10, U11, U12) to sensor circuit voltage output entering DVM based on
     # a normal distribution
     V_RTI = Vout
     V_RTI = V_RTI + randn(0, 1/1e6/2)
     V_RTI = V_RTI + randn(0, 5/1e6/2)
     V_RTI = V_RTI + randn(0, del_Temp_C * 1/1e6/2)
     V_RTI = V_RTI + randn(0, 1.5/1e6/2)
     # Amplify voltage by gain and add post-amplified uncertainties, or Referred to
     # Output (RTO) uncertainties (U13, U14, U15, U16) based on a normal distribution
     V_RTO = V_RTI * gain
     V_RTO = V_RTO + randn(0, 0.5/1e3/2)
     V_RTO = V_RTO + randn(0, 1/1e3/2)
     V_RTO = V_RTO + randn(0, del_Temp_C * 0.2/1e3/2)
     V_RTO = V_RTO + randn(0, 2/1e3/2)
     # Model digitizer uncertainties (U17, U18) based on a normal distribution,
     # and convert to 16-bit representation
     V_RTO = V_RTO * randn(1.0, 0.005/100/2)
     VPerCount = 20 / (2 ** 16)
     digitizedVoltage = round(V_RTO / VPerCount)
     digitizedVoltage = digitizedVoltage + round(randn(0,4/2))
     # Calculate the estimated measured voltage by converting to original
     # measurement scale
     V_meas = digitizedVoltage * VPerCount
     V_meas = V_meas/Gprog
     return V_meas
```

Figure 5. Simplified pseudocode for the modeling of the digital voltmeter function.

3.3 Laboratory Equipment Temperature

Changes in the DAS temperature influence the measurement performance. A change of 10 Fahrenheit degrees is considered the largest temperature variation to occur over long-duration testing in the NASA AFRC FLL; therefore, within the MCM, the laboratory temperatures were varied from $\Delta T = \pm 0, \pm 2, \pm 4, \pm 6, \pm 8$ and ± 10 Fahrenheit degrees. The resulting changes in temperature (ΔT) were converted from Fahrenheit to Celsius, then fed to the V_{source}, DVM, and BCM models.

These temperature changes can be a result of self-heating of electronics or environmental changes within the laboratory environment. It is also noted that changes in temperature resulting from self-heating of electronics are minimized with the implementation of standard FLL testing procedures, which require data acquisition electronics to run for an extended period of time before taking any measurements.

4 Measuring Strain with a Wheatstone Bridge Circuit

A Wheatstone bridge circuit is used to monitor strain from a bonded metallic-foil grid resistance strain gage. A Wheatstone bridge circuit is used to provide relatively large changes in voltage for small changes in resistance. An example of a single active arm (or "quarter-bridge") Wheatstone bridge circuit is shown in figure 6.

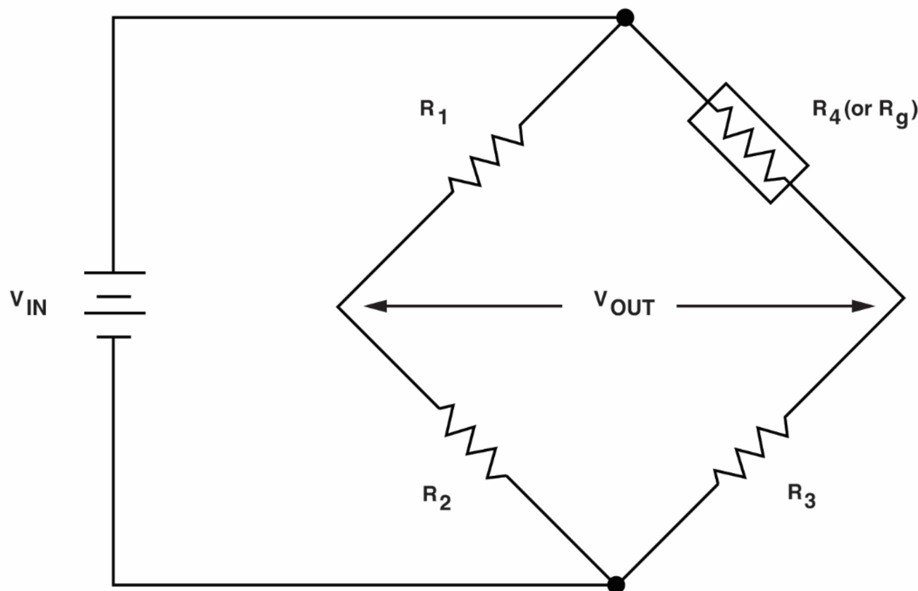

Figure 6. Quarter-bridge Wheatstone circuit.

All Wheatstone bridge circuits will contain four resistors (R_1, R_2, R_3, and R_4 (or R_g)) electrically arranged in the pattern shown in figure 6. Every resistance in the circuit can either come from active foil strain gages or bridge completion resistors provided by the DAS, as discussed in section 4.1. The bridge completion resistors should match the base strain-gage resistance as closely as is practical. A commonly used strain-gage resistance value in the FLL is 350 ohm (Ω). A measurement from the Wheatstone bridge circuit is obtained by comparing input excitation voltage (V_{in}) and voltage potential from a junction between R_1 and R_2 to a junction between R_4 and R_3 (V_{out}). Reference 5 presents further information regarding the Wheatstone bridge circ uit.

Input voltage is then passed to the $V_{source}( )$ function to include uncertainty of the excitation voltage. Output voltage for all strain-gage Wheatstone bridge circuits is shown in equation (1).

$$V_{out} = V_{Source}(V_{in}) \cdot \left[\frac{R_3}{R_3 + R_4} - \frac{R_2}{R_1 + R_2}\right] \quad (1)$$

The difference of the ratios of input and output voltage, measured at the strained and unstrained state (V_r), is defined in equation (2). The FLL DAS does not monitor input voltage, so V_{in} does not get processed by the DVM( ) function. The Wheatstone bridge circuit voltage output V_{out} from equation (1) is passed into equation (2). Since output voltage is measured by the DAS, output voltage is processed through the DVM( ) function, as previously described in section 3.2.

$$V_r = \left[\left(\frac{DVM(V_{out})}{V_{in}}\right)_{strained} - \left(\frac{DVM(V_{out})}{V_{in}}\right)_{unstrained}\right] \quad (2)$$

4.1 Bridge Completion Model

As stated in section 4, all Wheatstone bridge circuits require four resistive elements. Depending on the type of strain-sensing circuit, the BCM within the DAS can supply two (for half-bridge) or three (for quarter-bridge) circuits of the resistive elements to complete the Wheatstone bridge circuit. All bridge completion resistors are assumed to have the same targeted resistance (R_i) as the strain-gage resistance. Assumed uncertainties for the bridge completion resistors are borrowed from uncertainties reported for a Vishay Model P3 (Vishay Micro-Measurements) (Raleigh, North Carolina) Strain Indicator and Recorder (ref. 4).

Additionally, resistance uncertainties based on temperature changes are borrowed from example data provided by Hewlett-Packard (Hewlett-Packard Company) (Palo Alto, California), "Practical Strain Gage Measurements" (ref. 5). In the BCM, a base resistance based on a random value from a normal distribution is obtained for each bridge completion resistor (R_1, R_2, and R_3). A temperature based on the changes in the DAS temperature is then applied to all the bridge completion resistors for a strained state, as previously discussed in section 3.3. The bridge completion resistor uncertainties (U19 and U20) are shown in table 1. Example pseudocode for the BCM function is shown in figure 7. The BCM model outputs a resistance for the unstrained and strained state. Because the unstrained state is the reference state for the measurement, it is assumed that there is no temperature uncertainty for this state.

```
# Example pseudo-code, Bridge Completion Model
# Estimate the bridge completion resistors based all uncertainties (U19, U20)
# Use a random number generator with normal distribution (randn).
# The randn function has two inputs, the mean and the standard deviation
# randn(mean, standard deviation)
def BCM(Ri, del_Temp_C):
        # Estimate bridge completion resistors based on base resistance.
        # Apply uncertainties (U19 and U20) based on a normal distribution
        # Ri_Unstrained has no temperature change
        Ri = Ri * randn(1.0, 0.01/100/2)
        Ri_Unstrained = Ri
        Ri_Strained = Ri * randn(1.0, del_Temp_C * 3.1e-6/2)
        return Ri_Unstrained, Ri_Strained
```

Figure 7. Example pseudocode for the bridge completion model function.

4.1.1 *Wheatstone Bridge, Single Active Arm (Quarter-bridge Circuit)*

A single active arm (quarter-bridge) is a Wheatstone bridge circuit where only one of the four resistors is an active strain gage. Figure 8 shows an example of a quarter-bridge circuit with lead wire resistances (R_ℓ) included.

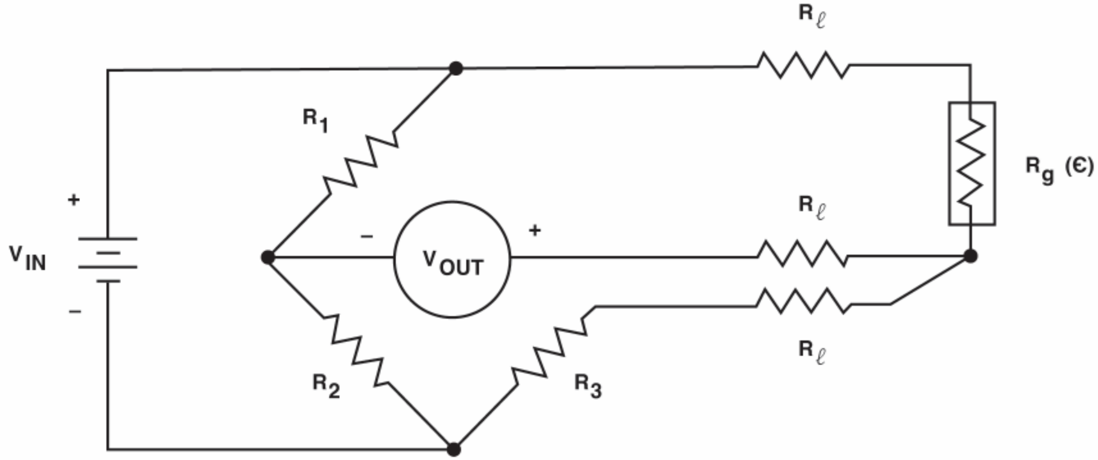

Figure 8. Quarter-bridge Wheatstone circuit with lead-wire resistance.

The circuit in figure 8 depicts three bridge completion resistors (R_1, R_2, and R_3) that are insensitive to strain, and the foil strain gage (R_g) that is the only resistor in the system that changes relative to strain. For the strain-g model, the three bridge completion resistors are all subjected to the perturbations introduced in table 1.

Lead-wire resistance (R_ℓ) is taken into account as additional resistance in the system. When the DVM has high impedance (as is the case with the DAS), very limited current flows through V_{out}; therefore, the in-line lead-wire resistance is neglected in the V_{out} leg.

To measure strain from a foil strain gage, it is necessary to obtain the gage factor (GF) of the strain gage, which relates changes in resistance to strain. The gage factor will be provided by the strain-gage vendor upon delivery. The relationship between the changes in resistance to change in strain is shown in equation (3).

$$GF = \frac{\Delta R_g / R_g}{\varepsilon} \tag{3}$$

Given a gage factor of a strain gage and the circuit in figure 8, it is possible to calculate strain from monitoring the voltage difference ratio (V_r) from equation (2). Equation (4) (ref. 5) is used to calculate strain (ε) without taking into account the lead-wire resistance (R_ℓ).

$$\varepsilon = \frac{-4V_r}{GF(1 + 2V_r)} \tag{4}$$

When the lead-wire resistance (R_ℓ) is considered, an additional lead-wire resistance coefficient (C_ℓ) is included. Both lead-wire resistance (R_ℓ) and strain-gage resistance (R_g) are measured with an ohmmeter, independent of the DAS while the test article is unstrained.

$$C_\ell = \left(1 + \frac{R_\ell}{R_g}\right) \tag{5}$$

The lead-wire resistance is taken into account for both quarter-bridge and half-bridge circuits, as discussed in section 4.2. The updated quarter-bridge strain equation (equation 6), with lead-wire resistance (ref. 5) accounted for, becomes:

$$\varepsilon = \frac{-4V_r}{GF(1+2V_r)} \cdot C_\ell \tag{6}$$

4.1.2 Wheatstone bridge, half-bridge circuit

A Wheatstone bridge, half-bridge circuit is a strain-sensing circuit where two adjacent resistor legs of a Wheatstone bridge are foil strain gages, and the two remaining resistors (R_1 and R_2) are bridge completion resistors that are insensitive to strain. For the BCM( ), the two bridge completion resistors are subjected to the perturbations (U19, U20) and are introduced in table 1 and section 4.1.

Depending on the physical placement of the two foil strain gages, the resulting change in voltage to strain equation will vary. The circuitry of the half bridge is independent of the physical location of the strain gage. Examples of the half-bridge circuity for both Half-bridge, Type-I (HB-T-I) and Half-bridge, Type-II (HB-T-II) are shown in figure 9 and discussed in sections 4.1.2.1 and 4.1.2.2, respectively.

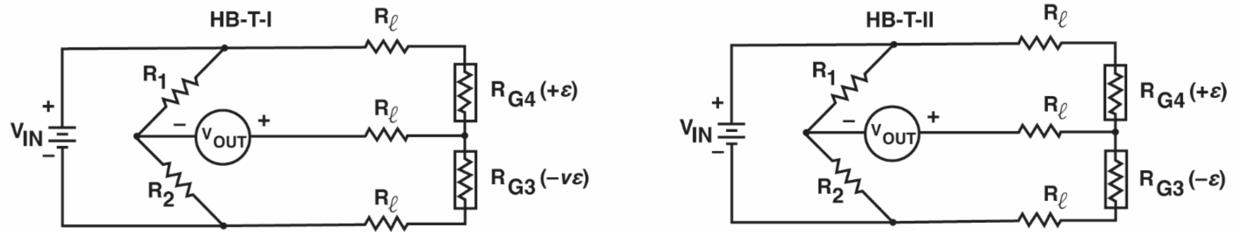

Figure 9. Half-bridge circuits: (left) Half-bridge, Type-I; and (right) Half-bridge, Type-II.

4.1.2.1 Half-bridge, Type-I – For this report, a Half-bridge, Type I (HB-T-I) circuit is defined when the two active strain gages are as follows: 1) on the same surface; 2) are physically located adjacent to one another; and 3) gage directions are perpendicular to one another. An example of the physical placement of the strain gages in an HB-T-I configuration, applied to a beam, is shown in figure 10. Although there are two strain gages in the circuit, there is only one resulting strain measurement extracted from the circuit. When applied to a beam, the HB-T-I configuration is sensitive to both axial strain and bending strain experienced on the surface of a test article. Also, the close proximity of the two gages allows for localized temperature compensation. As well, the combination of perpendicular strain gages helps to compensate for the Poisson effect of the structure being measured. The voltage to strain equation for HB-T-I is shown in equation (7), where ν is the Poisson ratio of the structural material being measured. The difference ratio (V_r) from equation (2) is updated with R_3 (replaced by R_{G3}), and R_4 (replaced by R_{G4}).

$$\varepsilon = \frac{-4V_r}{GF[(1+\nu) - 2V_r(\nu - 1)]} \cdot C_\ell \tag{7}$$

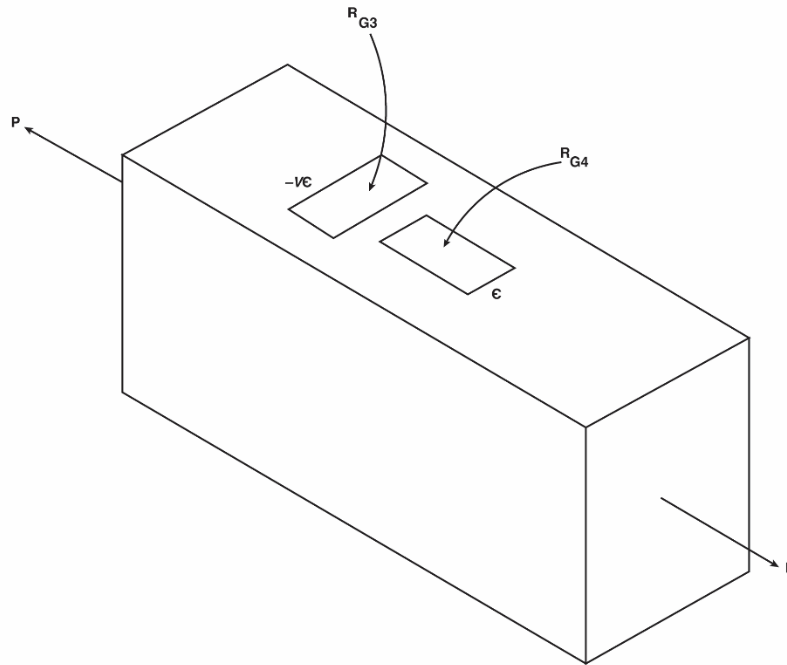

Figure 10. Half-bridge, Type-I.

4.1.2.2 Half-bridge, Type-II – Within this report, a Half-bridge, Type II (HB-T-II) circuit is defined when the two strain gages are as follows: 1) physically located on different surfaces (e.g., top and bottom) of a structure; and 2) gage directions are parallel. Figure 11 shows an example of the physical placement of the strain gages in an HB-T-II configuration on a beam. When applied to beams, the HB-T-II configuration is only sensitive to bending strain experienced by the two opposite surfaces of a test article. The change in voltage to strain equation for HB-T-II is shown in equation (8). The difference ratio (V_r) from equation (2) is updated with R_3 (replaced by R_{G3}), and R_4 (replaced by R_{G4}).

$$\varepsilon = \frac{-2V_r}{GF} \cdot C_\ell \tag{8}$$

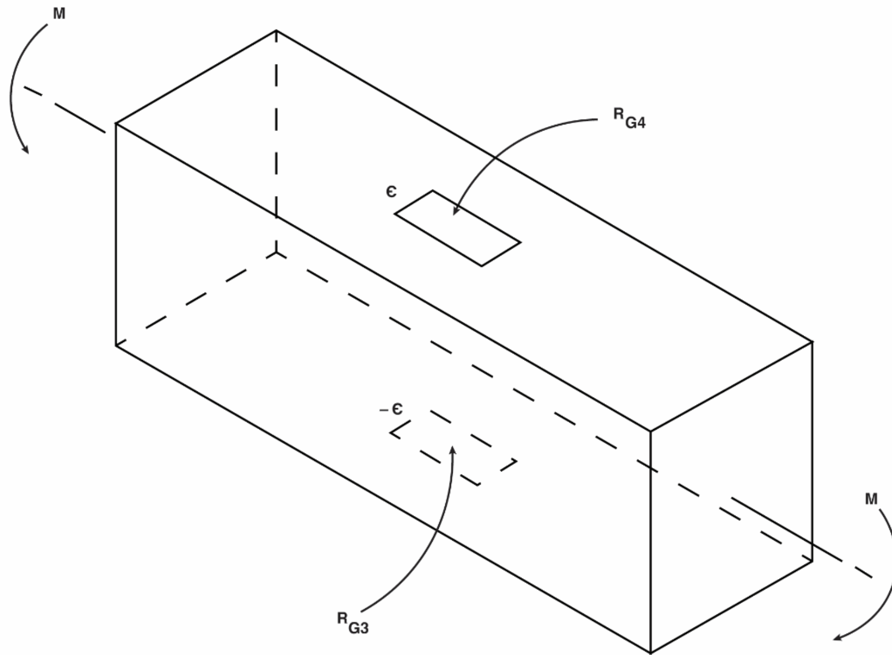

Figure 11. Half-bridge, Type-II.

4.1.3 Wheatstone Bridge, Full-bridge Circuit

A Wheatstone bridge, full-bridge circuit is a strain-sensing circuit where all four resistors are active strain gages; therefore, there are no bridge completion resistors. Depending on the physical placement of the four strain gages, the resulting change in voltage to strain equation will vary. The circuitry of the full bridge is independent of the physical location of the strain gage. An example of the full-bridge circuity for all Full-bridge, Type-I (FB-T-I); Full-bridge, Type-II (FB-T-II); and Full-bridge, Type-III (FB-T-III) circuits are shown in figure 12. Further information on FB-T-I, FB-T-II, and FB-T-III is provided in sections 4.1.3.1, 4.1.3.2, and 4.1.3.3, respectively. Note: the lead-wire resistance (R`) is not included in figure 12. When installing the strain gages, it is important to keep all lead wires the same length such that the lead-wire resistances are all equal. When all lead wires have equal resistance, there is no need to take lead-wire resistance into account for all full-bridge circuit equations.

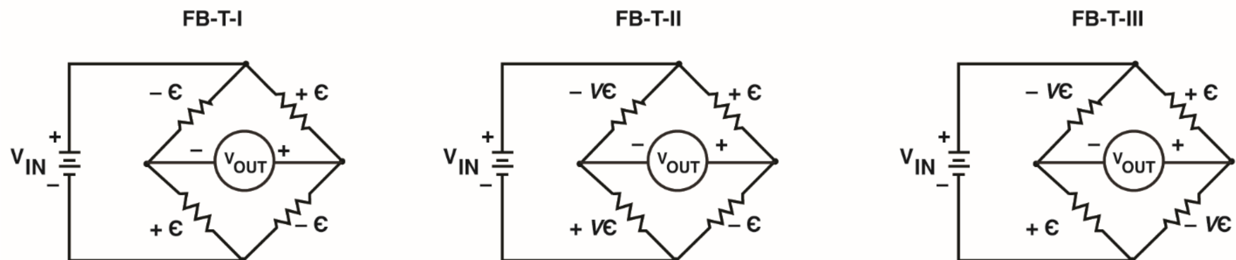

Figure 12. Full-bridge circuit (Type-I, Type II, and Type III).

4.1.3.1 Full-bridge, Type-I – When a Full-bridge, Type-I (FB-T-I) circuit is applied to a beam, the circuit can be used to either monitor bending strains or torsional strains, depending on the physical locations of the four active strain gages. When used to monitor bending strain, a FB-T-I circuit is defined as follows: 1) when all four legs of a Wheatstone bridge circuit are active strain gages; 2) two of the four strain gages are physically adjacent; 3) all four strain gages are aligned in parallel to one another on a common surface (e.g., top surface); 4) the other remaining two strain gages are physically adjacent 5) are aligned in parallel on the opposite surface (e.g., bottom surface); and 6) within the Wheatstone bridge circuitry, each pair (adjacent and parallel) of strain gages are on opposite legs, and with neither gage containing nodes in direct connection, as previously shown in figure 12. An example of the physical placement of the strain gages in an HB-T-I bending configuration is shown in figure 13.

When used to monitor torsion strain, a FB-T-I circuit is defined as follows: 1) when all four legs of a Wheatstone bridge circuit are active strain gages; 2) two of the four strain gages are physically adjacent; 3) all four legs are aligned at a ±45-degree offset relative to the torsional axis; 4) all four legs are aligned perpendicular to one another on a common surface (e.g., top surface); 5) the other remaining two strain gages are physically adjacent; 6) all four legs are aligned at a ±45-degree offset relative to the torsional axis; 7) all four legs are aligned perpendicular to one another on a common surface (e.g., bottom surface); and 8) all four legs are within the Wheatstone bridge circuitry, each pair of physically adjacent and perpendicular strain gages are on adjacent legs, as previously shown in figure 12. An example of the physical placement of the strain gages in an HB-T-I torsion configuration is shown in figure 13.

Additional sensor placement configurations exist; however, this circuit configuration is what defines the FB-T-I configuration. For either the bending or torsional configuration of FB-T-I, the voltage to strain equation will be the same. The voltage to strain equation for an FB-T-I configuration is shown in equation (9). The difference ratio (V_r) from equation (2) is updated with R_1 (replaced by R_{G1}); R_2 (replaced by R_{G2}); R_3 (replaced by R_{G3}); and R_4 (replaced by R_{G4}).

$$\varepsilon = \frac{-V_r}{GF} \tag{9}$$

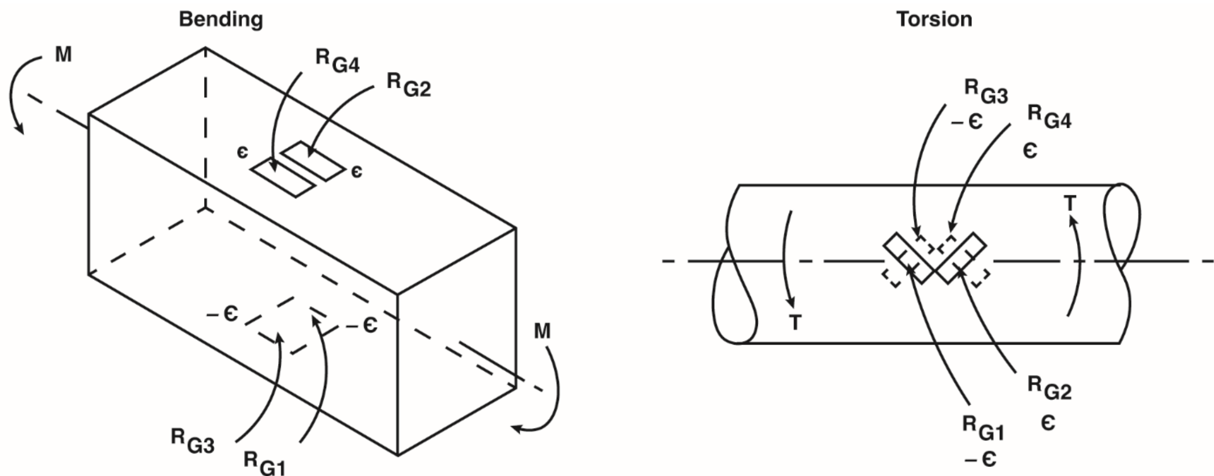

Figure 13. (left) Full-bridge, Type-I on a surface under bending; and (right) torsion.

4.1.3.2 Full-bridge, Type-II – A Full-bridge, Type-II (FB-T-II) circuit is used to exclusively monitor bending strains based on the physical locations of the four active strain gages. The FB-T-II circuit is defined as follows: 1) when all four legs of a Wheatstone bridge circuit are active strain gages; 2) two of the four strain gages are physically adjacent; 3) all strain gages are aligned perpendicular to one another on a common surface (e.g., top surface); 4) the other remaining two strain gages are physically adjacent; 5) all strain gages are aligned perpendicular to one another on the opposite surface (e.g., bottom surface); 6) one pair of parallel strain gages from an opposite surface are aligned in the direction of bending strain; 7) the other pair of parallel strain gages from opposite surfaces are aligned to monitor the Poisson effect; and 8) within the Wheatstone bridge circuitry, each parallel strain gage from opposite surfaces are on adjacent legs, as previously shown in figure 12. An example of the physical placement of the strain gages in an FB-T-II bending configuration is shown in figure 14. The voltage to strain equation for an FB-T-II configuration is shown in equation (10). The difference ratio (V_r) from equation (2) is updated with R_1 (replaced by R_{G1}); R_2 (replaced by R_{G2}); R_3 (replaced by R_{G3}); and R_4 (replaced by R_{G4}).

$$\varepsilon = \frac{-2V_r}{GF(\nu + 1)} \qquad (10)$$

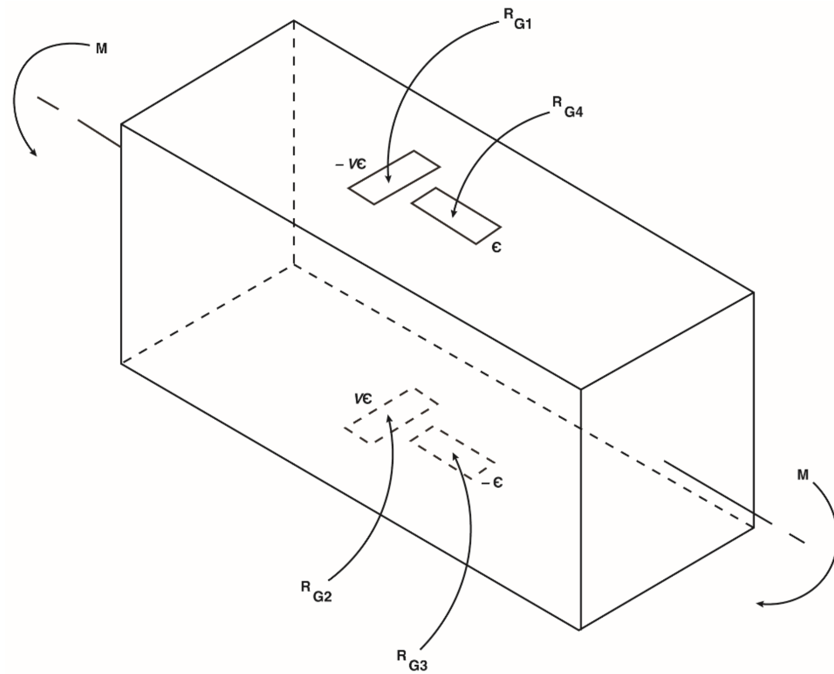

Figure 14. Full-bridge, Type-II.

4.1.3.3 Full-bridge, Type-III – A Full-bridge, Type-III (FB-T-III) circuit is used, exclusively, to monitor axial strains based on the physical locations of the four active strain gages. The FB-T-III circuit is defined as follows: 1) when all four legs of a Wheatstone bridge circuit are active strain gages; 2) two of the four strain gages are physically adjacent; 3) all four legs are aligned perpendicular to one another on a common surface (e.g., top surface); 4) the other remaining two strain gages are physically adjacent; 5) all four legs are aligned perpendicular to one another; 6) all four legs are on the opposite surface (e.g., bottom surface); 7) one pair of parallel strain gages from opposite surfaces are aligned in the direction of axial strain; 8) the other pair of parallel strain gages from opposite surfaces are aligned to monitor the Poisson effect; and 9) within the Wheatstone bridge circuitry, each pair of strain gages on a common surface are on adjacent legs, as previously shown in figure 12. An example of the physical placement of the strain gages in a FB-T-III axial configuration is shown in figure 15. The voltage to strain equation for an FB-T-III configuration is shown in equation (11). The difference ratio (V_r) from equation (2) is updated with R_1 (replaced by R_{G1}); R_2 (replaced by R_{G2}); R_3 (replaced by R_{G3}); and R_4 (replaced by R_{G4}).

$$\varepsilon = \frac{-2V_r}{GF[(\nu + 1) - Vr(\nu - 1)]} \tag{11}$$

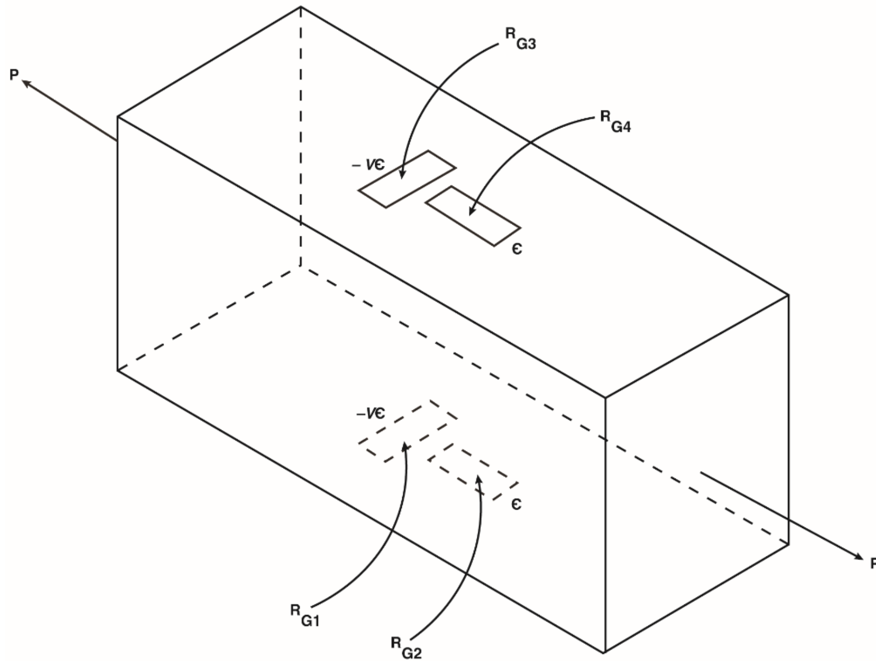

Figure 15. Full-bridge, Type-III.

4.2 Strain Measurement Model

All foil strain-gage types within this report are modeled using a Wheatstone bridge circuit. Depending on the type of strain-gage configuration (quarter-bridge, half-bridge, or full-bridge), the BCM will supply the appropriate number of bridge completion resistors with included uncertainties, as previously discussed in section 4.1. Once all resistors are modeled, the process of modeling a strain measurement will be the same for all strain-gage configuration types, with the only difference being that the voltage to strain equation is applied after the voltage measurements are obtained. A summary of the voltage to strain

equations are shown in table 2. An example flow chart of the strain-gage measurement model is shown in figure 16. User programmable inputs to the DAS include V_{in}, G_{prog}, the strain-gage configuration, gage factor, the base resistance values (R_i), and the change in the ambient temperature. The strain measurement flow chart includes the voltage excitation source model (V_{source}); bridge completion model (BCM); and the digital voltmeter (DVM) model.

Table 2. Voltage to strain equations for various bridge types.

Bridge type	Strain equation
Quarter-bridge	$\varepsilon = \dfrac{-4V_r}{GF(1+2V_r)} C_\ell$
Half-bridge, Type I	$\varepsilon = \dfrac{-4V_r}{GF[(1+\nu)-2V_r(\nu-1)]} C_\ell$
Half-bridge, Type-II	$\varepsilon = \dfrac{-2V_r}{GF} C_\ell$
Full-bridge, Type-I	$\varepsilon = \dfrac{-V_r}{GF}$
Full-bridge, Type-II	$\varepsilon = \dfrac{-2V_r}{GF(\nu+1)}$
Full-bridge, Type-III	$\varepsilon = \dfrac{-2V_r}{GF[(\nu+1)-V_r(\nu-1)]}$

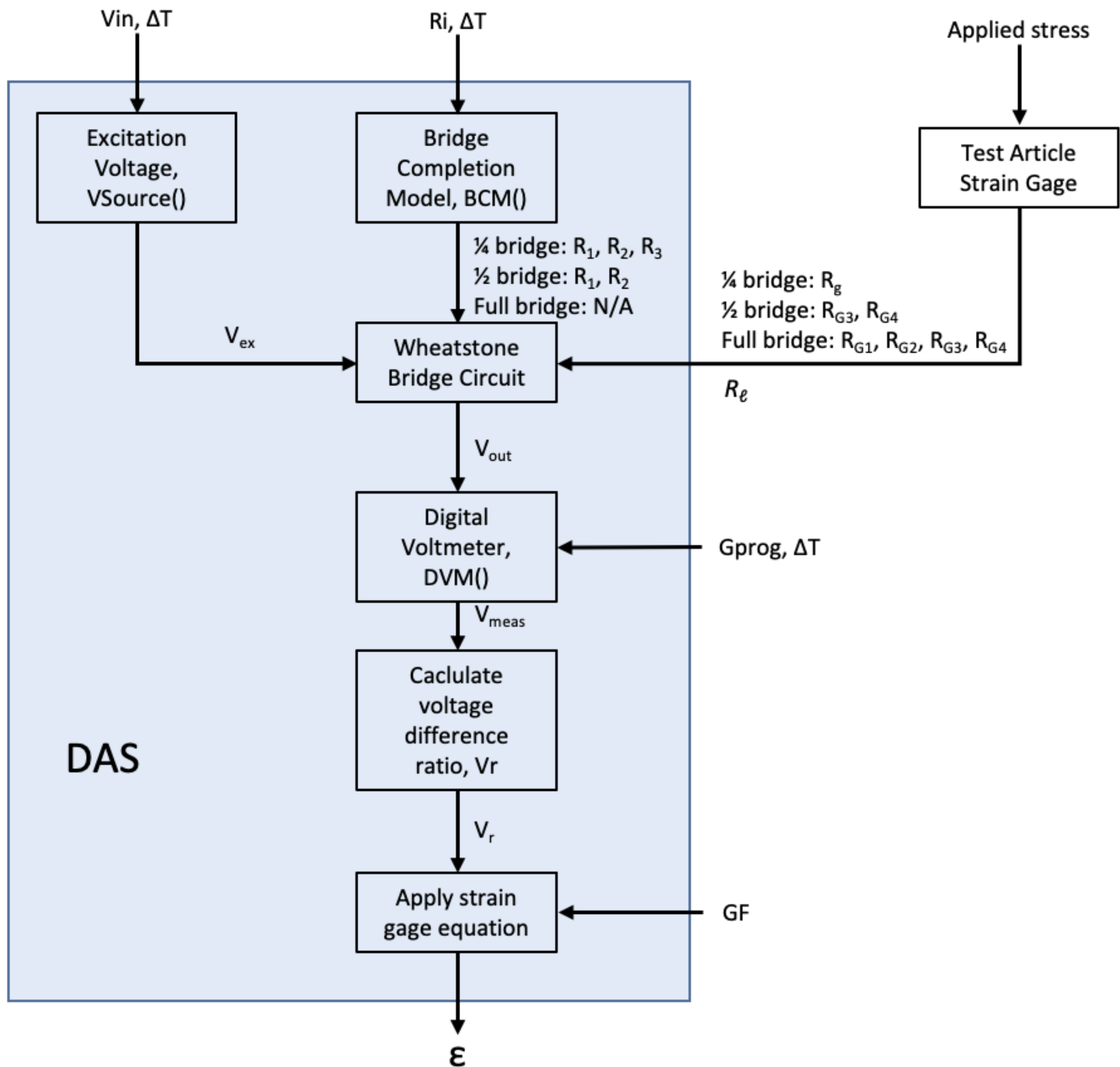

Figure 16. Strain-gage measurement model flowchart.

4.3 Monte Carlo Simulation Results for a Strain Measurement Model

A Monte Carlo simulation was conducted for all strain-gage configuration types to estimate the measurement uncertainty of a representative DAS, used in the FLL. The strain measurement model consisted of both the DAS component models, shown in section 3, and the strain sensor model, as previously shown in figure 16. For these simulations, the lead-wire resistance ($R\ell$) was set to zero. For all configurations, a gage factor of GF = 2.0, and an unstrained gage resistance of 350 Ω was modeled. The gage factor and gage resistance have their own uncertainties; however, the goal of this report was to estimate the uncertainty of an isolated DAS, so the strain-gage variance was removed from the Monte Carlo analysis.

A common method to check the DAS strain measurement functionality is to use a strain-gage simulator (or "decade box") in place of a foil strain gage. A decade box is a device that enables a user to

set resistance outputs with relatively high accuracy (~0.02 percent of setting) to simulate the resistance of a foil strain gage. Although out of scope of this report, to enable quick verifications of the measurement uncertainties through testing with a decade box, the resulting measurement uncertainties are provided in increments of 0.5 ohm for gages aligned in the axial direction, which is approximately 714 microstrain (u_ε) increments. Where applicable (HB-T-I, FB-T-II, FB-T-III), an assumed Poisson ratio of the test article material is set to 0.32; therefore, the simulated transverse-aligned strain gages are increased in increments of 0.16 ohm.

A strain range over ±5,000 microstrain is considered a sufficient range to cover most common foil strain-gage measurements to be obtained in the FLL; therefore, for all strain-gage configurations, an axial strain range of ±5,714 microstrain is analyzed, which corresponds to a change in strain-gage resistance of ΔR_G = ±4.0 ohm, and ±1.28 ohm for transverse strain-gage resistance (where applicable) for all strain gage configurations.

Within the Monte Carlo simulation, the laboratory temperatures were varied for ΔT = ±0, ±2, ±4, ±6, ±8, and ±10 Fahrenheit degrees. Software programmable values such as the excitation voltage (V_{in}) and gain (G_{prog}) were held constant. The Monte Carlo simulation uses typical settings used in the FLL for strain-gage measurements, which include setting the excitation voltage (V_{in}) to 5.0 volt; the G_{prog} (for quarter-bridge and half-bridge configurations) set to 300; and the gain set to 150 for all full-bridge configurations. A full-bridge circuit has increased sensitivity to strain; therefore, the gain is lowered to prevent saturation of the DVM over the desired strain range. Each gage resistor setting for each strain-gage configuration was processed for 50,000 iterations from which the two-standard deviations uncertainty of the measurement uncertainty was estimated (i.e., a 95-percent level of confidence). At this point, a comment must be made about convergence of the Monte Carlo simulations. While a specific convergence criterion was not established for each run of the Monte Carlo simulation in this report, it was clear from the results that the curves produced by the Monte Carlo simulations are very smooth as opposed to noisy and jagged (as a set of poorly converged simulations would appear when plotted). For example, the curves generated for the half-bridge configuration in figure 17 are rather smooth and continuous, and from a practical point of view, if an engineer were to use this plot to estimate the uncertainty in measurement, they would pick a value from the figure by hand. The uncertainty in the process of using the human eye to estimate a value from the figure that would swamp the precision gained by running the simulation many more iterations; therefore, for all practical purposes, the simulations have sufficiently converged. A summary of the configurations for all the Monte Carlo simulation of strain measurement models is shown in table 3.

Table 3. Monte Carlo simulation strain-gage configuration.

Bridge Type	V_{in}	G_{prog}	GF	ν	ΔT (°F)	R1 (Ω)	R2 (Ω)	R3 (Ω)	R4 (Ω)
Half-bridge	5.0	300	2.0	N/A	0, 2, 4, 6, 8, 10	350	350	350	350, ±4
Half-bridge, Type-I	5.0	300	2.0	0.32	0, 2, 4, 6, 8, 10	350	350	350, ±1.2	350, ±4
Half-bridge, Type-II	5.0	300	2.0	N/A	0, 2, 4, 6, 8, 10	350	350	350, ±4	350, ±4
Full-bridge, Type-I	5.0	150	2.0	N/A	0, 2, 4, 6, 8, 10	350, ±4	350, ±4	350, ±4	350, ±4
Full-bridge, Type-II	5.0	150	2.0	0.32	0, 2, 4, 6, 8, 10	350, ±1.2	350, ±1.2	350, ±4	350, ±4
Full-bridge, Type-III	5.0	150	2.0	0.32	0, 2, 4, 6, 8, 10	350, ±1.2	350, ±4	350, ±1.2	350, ±4

The following figures are Monte Carlo simulation output of the resulting two standard deviations strain measurement uncertainty estimates versus measured microstrain for all the strain configurations presented in table 3. All the simulations span a range of ±5,714 microstrain and a temperature change of 10 Fahrenheit degrees, Figure 17 shows the quarter-bridge Monte Carlo simulation results, with a bounding two standard deviations uncertainty of ±26 microstrain over the full range. An example histogram and probability density function for the quarter-bridge Monte Carlo simulation at a change in gage resistance of +4 ohm and a change in temperature of 10 Fahrenheit degrees, which corresponds to the bounded measurement uncertainty for the quarter-bridge analysis, is shown in figure 18.

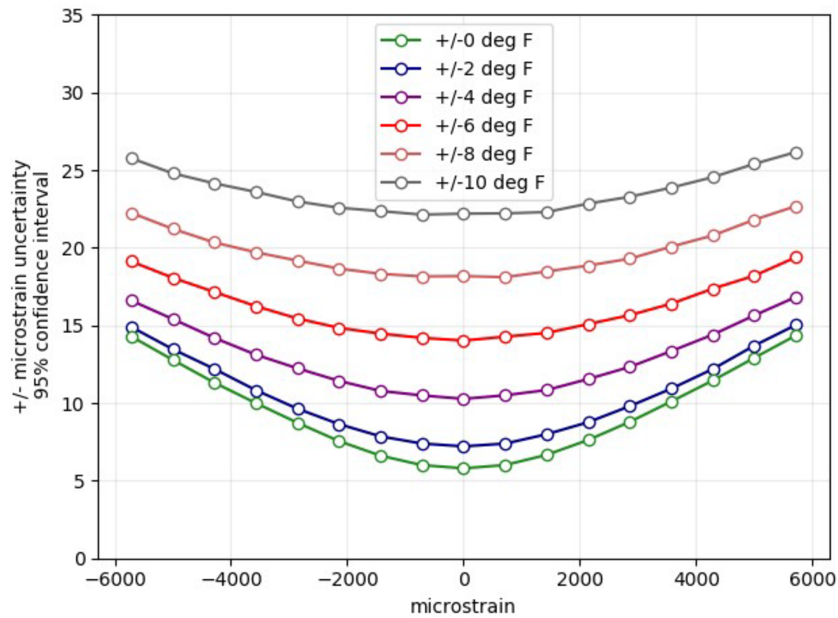

Figure 17. Quarter-bridge, two standard deviations Monte Carlo simulation results, V_{in} = 5.0 V, G_{prog} = 300.

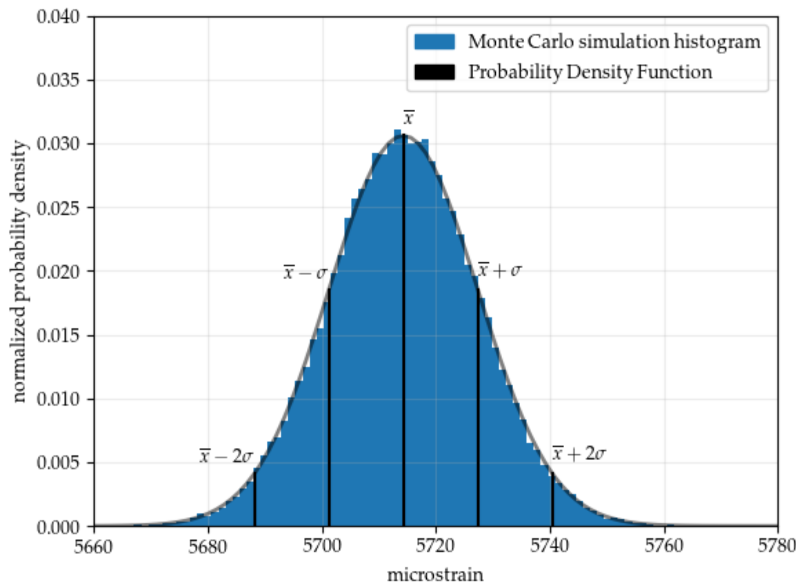

Figure 18. Quarter-bridge Monte Carlo simulation histogram and probability density function for ΔR_g = +4 Ω, ΔT = 10 °F, V_{in} = 5.0 V, G_{prog} = 300.

The Half-bridge (Type-I and Type-II) Monte Carlo simulation results are presented in figure 19 and figure 20, with a bounding two standard deviations uncertainty of ±20 for HB-T-I and ±17 for HB-T-II. It is noted that the temperature effects on the bridge completion resistors are not applicable to all full-bridge circuits since all the resistors in the circuit are active strain gages; therefore, there is significantly less measurement uncertainty due to temperature. Figure 21, figure 22, and figure 23 are the Monte Carlo simulation results for the Full-bridge (Type-I, Type-II, and Type-III), respectively. For all full-bridge strain configurations, the bounding two standard deviations uncertainty is ±15 microstrain over the full range. A summary of the bounding errors rounded up to the integer value for all strain-gage configurations is shown in table 4.

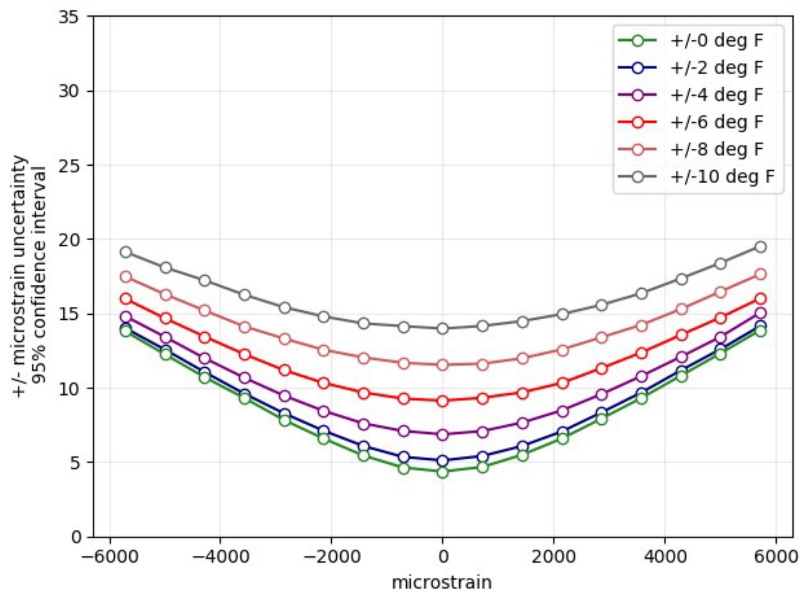

Figure 19. Half-bridge, Type-I, two standard deviations Monte Carlo simulation results, V_{in} = 5.0 V, G_{prog} = 300.

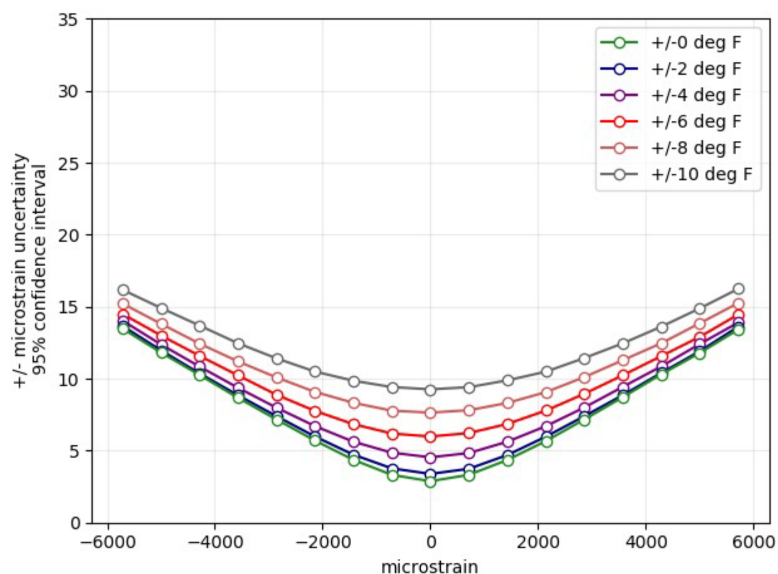

Figure 20. Half-bridge, Type-II, two standard deviations Monte Carlo simulation results, V_{in} = 5.0 V, G_{prog} = 300.

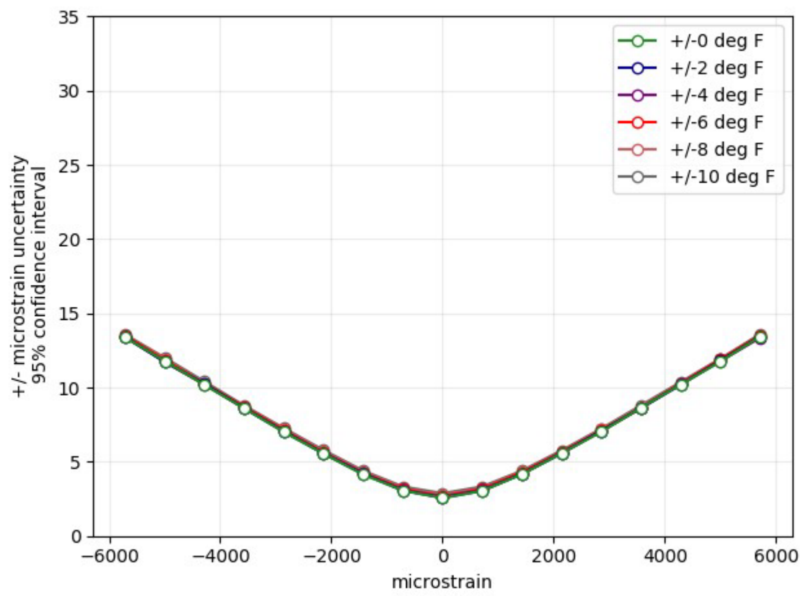

Figure 21. Full-bridge, Type-I, two standard deviations Monte Carlo simulation results, V_{in} = 5.0 V, G_{prog} = 150.

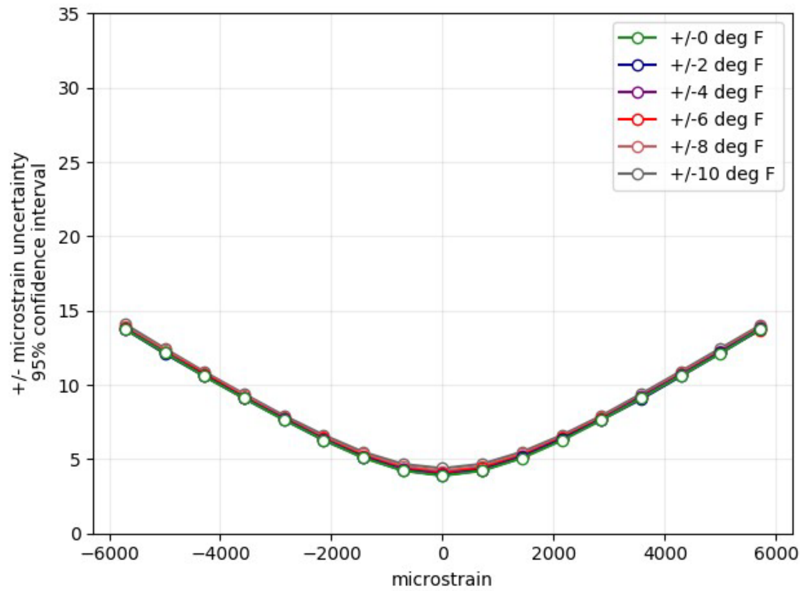

Figure 22. Full-bridge, Type-II, two standard deviations Monte Carlo simulation results, V_{in} = 5.0 V, G_{prog} = 150.

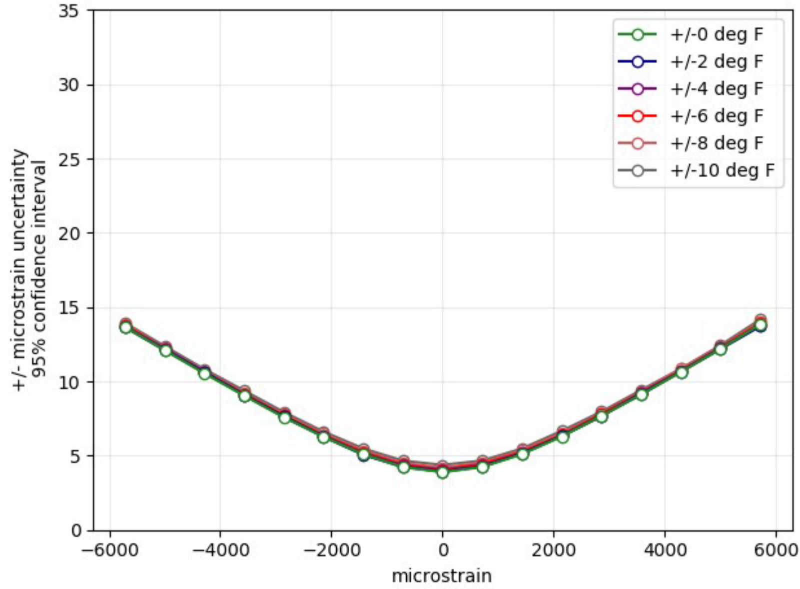

Figure 23. Full-bridge, Type-III, two standard deviations Monte Carlo simulation results, V_{in} = 5.0 V, G_{prog} = 150.

Table 4. Bounded measurement uncertainty for various strain gages.

Bridge type	V_{in}	Gain	Strain range	Ambient temperature change	Two standard deviations measurement uncertainty
Quarter-bridge	5.0	300	±5,714 με	10 °F	±26 με
Half-bridge, Type-I	5.0	300	±5,714 με	10 °F	±20 με
Half-bridge, Type-II	5.0	300	±5,714 με	10 °F	±17 με
Full-bridge, Type-I	5.0	150	±5,714 με	10 °F	±15 με
Full-bridge, Type-II	5.0	150	±5,714 με	10 °F	±15 με
Full-bridge, Type-III	5.0	150	±5,714 με	10 °F	±15 με

5 Load Cell Monte Carlo Simulation Results

A load cell is a sensor that converts applied force to a proportional voltage. The internal circuit of a load cell is equivalent to a Full-bridge, Type-I circuit, as previously discussed in section 4.3. Typical load cell sensitivity units are force per measured and millivolt per supplied excitation voltage. The DAS supplies the excitation voltage (V_{in}) and measures the full-bridge output voltage (V_{out}) in the same process as previously outlined in section 4. A typical DAS setting for load cells used in the FLL, include an excitation voltage (V_{in}) of 10 volt and a gain (G_{prog}) of 200. The underlying DAS measurement for a load cell is a measurement of millivolt per supplied excitation voltage.

The load cell measurement model flowchart is shown in figure 24. Inputs to the load cell model include the input voltage (V_{in}), (G_{prog}), the load cell sensitivity, and the change in the ambient temperature. The load cell measurement flow chart includes the voltage excitation source model (V_{source}) and the digital voltmeter model (DVM).

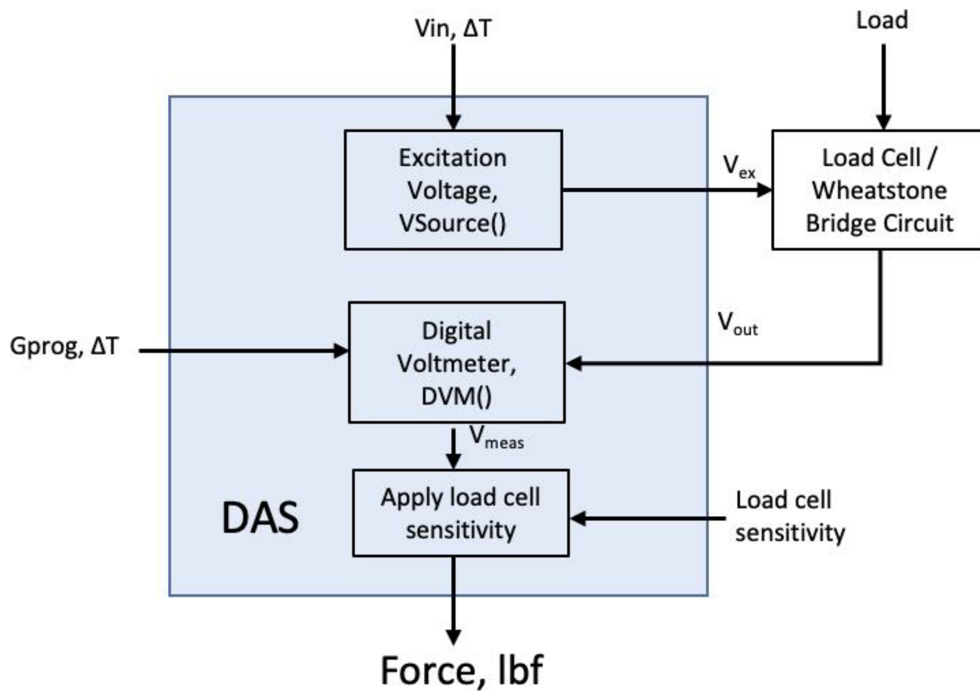

Figure 24. Load cell measurement model flowchart.

Figure 25 shows the Monte Carlo simulation results for the DAS measurement uncertainty for measured millivolt per supplied excitation voltage. The measurement uncertainty as a consequence of temperature is neglected since temperature has little effect on Full-bridge, Type-I strain gages, as shown in section 4.6.

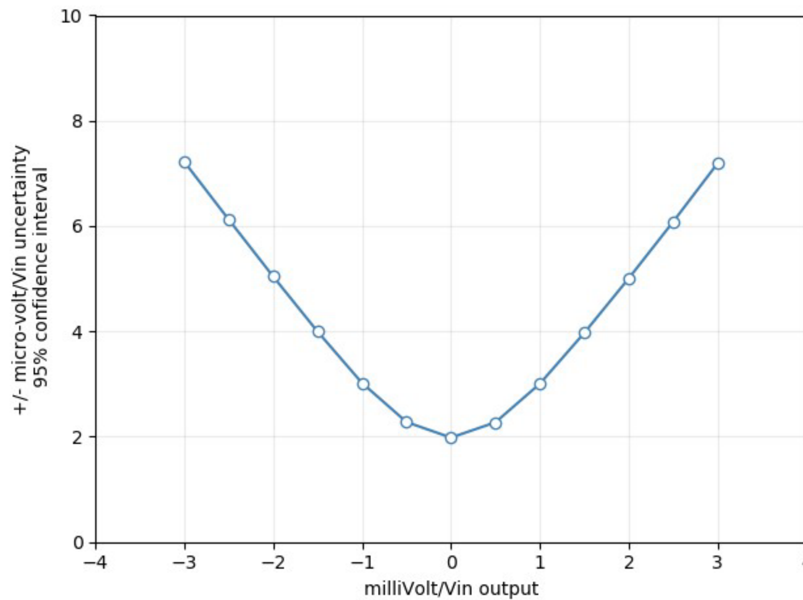

Figure 25. Measured millivolt per supplied excitation voltage, two standard deviations Monte Carlo simulation, V_{in} = 10.0 V, G_{prog} = 200.

The results shown in figure 25 can be used to estimate the measurement uncertainty for Full-bridge, Type-I load cells as long as the sensitivity settings are incorporated. The bounded uncertainty of measured millivolt per supplied voltage over a range of ±3 mV/V_{in} is ±7.2 µV/V_{in}. The measured millivolt per supplied excitation voltage measurement uncertainty can be scaled by the sensitivity of the load cell. Various load cell capacities are available commercially. Typical load cell capacities used in the NASA AFRC FLL include, but are not limited to 100, 1,000, 10,000, and 100,000 pounds. A load cell is selected based on the anticipated load range to be measured.

As an example, assuming a 100,000-pound capacity load cell is selected, a typical sensor sensitivity would be approximately 100k lbf/3 mV/V_{in} (depending on the design of the load cell). The estimated bounded uncertainty of a voltage measurement of ±7.2 µV/V_{in} can be multiplied by the load cell sensitivity of 100k lbf/3 mV/V_{in} to estimate the bounded measurement uncertainty of load, which is 240 lbf (±7.2 µV/V_{in} × 100k lbf/3 mV/V_{in} = ±240 lbf). An example of the measurement uncertainty for a 100,000-pound load cell is shown in figure 26. An example of typical load cell bounded uncertainties for various load cell capacities is shown in table 5.

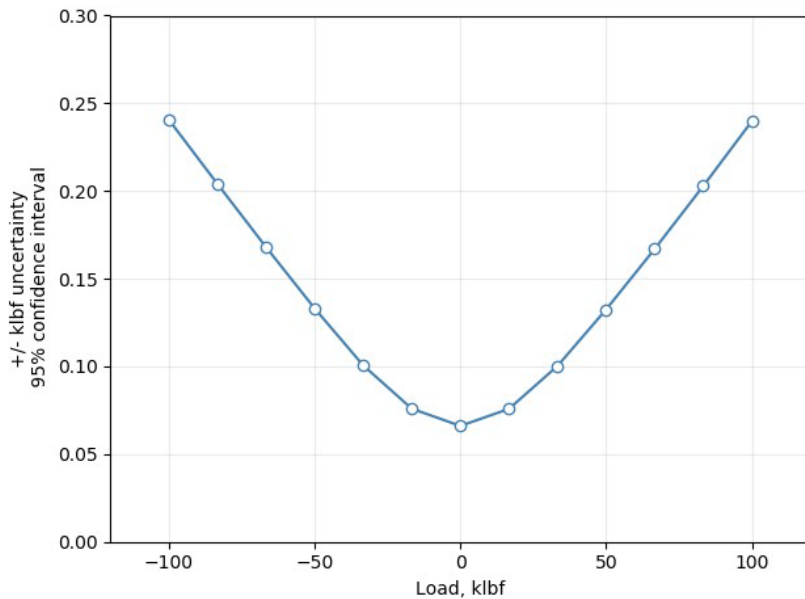

Figure 26. A 100,000-pound capacity load cell, two standard deviations Monte Carlo measurement uncertainty, sensitivity = 100k lbf/3 mV/V_{in}, V_{in} = 10.0 V, G_{prog} = 200.

Table 5. Bounded measurement uncertainty for various load cell capacities.

Load cell capacity	V_{in}	G_{prog}	Example load cell sensitivity	Two standard deviations measurement uncertainty
100 lbf	10.0 V	200	100 lbf/3 mV/V_{in}	0.24 lbf
1,000 lbf	10.0 V	200	1k lbf/3 mV/V_{in}	2.4 lbf
10,000 lbf	10.0 V	200	10k lbf/3 mV/V_{in}	24.0 lbf
100,000 lbf	10.0 V	200	100k lbf/3 mV/V_{in}	240 lbf

The example Monte Carlo simulation results provided in figure 26 and table 5 are based on voltage measurement uncertainties of the DAS. There are additional sensor-based measurement uncertainties. Typical additional errors can include strain-gage misalignment inside the load cell, sensor self-heating, and misalignment of load introduction into the load cell axis. Load cell calibration sheets may specify additional nonlinearity errors and hysteresis.

6 Monte Carlo Thermocouple Measurement Simulation Results

A thermocouple (TC) is a self-powered sensor that produces a voltage based on the Seebeck effect. The Seebeck effect occurs when wires of two different metals are joined together and exposed to a temperature differential relative to the end of the wires attached to the DAS. A typical TC circuit is shown in figure 27, where the desired temperature measurement is made at the junction of Metal A and Metal B (J_1). For most test setups, there is a need to transition from the thermocouple wire located on the test article to copper lead wires that are integrated in the test facility DAS. The transition is done at an isothermal block, as shown in J_3 and J_4 of figure 27. The additional junctions, however, where the TC wires transition to copper lead wires, create additional voltages because of the Seebeck effect. To account for the Seebeck voltages at J_3 and J_4, an isothermal block is used with the temperature of the isothermal block monitored. Typically, a resistance temperature detector (RTD) is employed to measure the temperature of the isothermal block. An RTD sensor can be used to obtain a more accurate temperature measurement than a TC but does not have the same range. Reference 6 provides more information regarding the design of a thermocouple circuit. Figure 28 shows an example of TC response curves (temperature versus voltage) for multiple TC types.

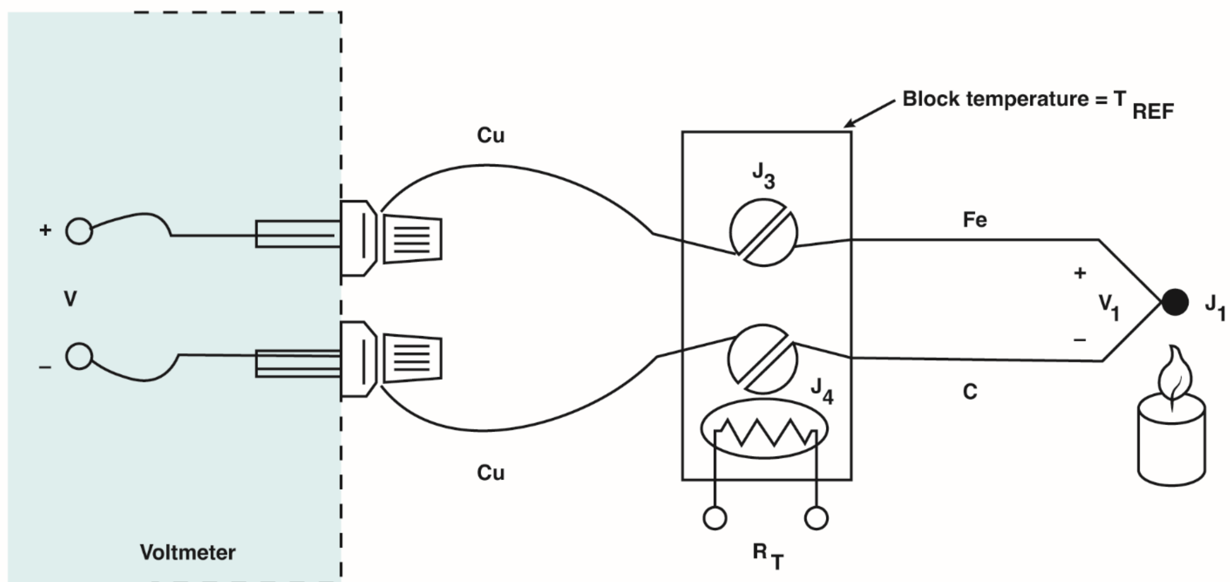

Figure 27. Thermocouple circuit with external reference junction (ref. 6).

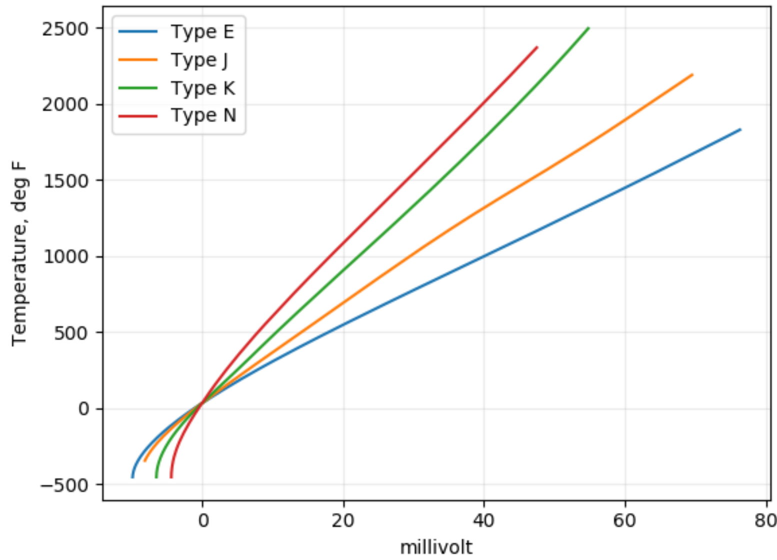

Figure 28. Typical thermocouple response curves, thermocouple Types (E, J, K, and N).

A Type-K thermocouple is commonly used in the AFRC FLL and is made from chromel and alumel and has an approximate sensitivity slope of α = 41 µV/ºC. Increased accuracy can be obtained by using an official response curve of a Type-K thermocouple, from the National Institute of Standards and Technology (NIST) (U.S. Department of Commerce) (Gaithersburg, Maryland), that does not have a constant slope (ref. 7). To measure temperature with the circuit, shown in figure 27, the first step is to measure the temperature at the isothermal block (T_{ref}) by measuring the voltage at the isothermal block (V_{ref}). The second step is to obtain the output voltage (V_{out}), as shown in equation 12, and pass it to the DVM( ) function from section 3.2, as shown in equation 13; then, the following equations can be used to solve for the temperature at junction 1 (T_{J1}):

$$V_{out} = V_{J1} - V_{ref} \approx \alpha(T_{J1} - T_{ref}) \tag{12}$$

$$T_{J1} = T_{ref} + \frac{DVM(V_{out})}{\alpha} \tag{13}$$

It is assumed that the RTD temperature measurement has greater accuracy than the TC temperature measurement; therefore, for the Monte Carlo simulation, no additional measurement uncertainty was added to T_{ref}. Statistically, adding individual components of uncertainty to a system is incorporated as the root sum square of all contributing components. If the RTD has significantly less uncertainty, it will contribute very little to the overall system uncertainty. The TC sensitivity (α) is a function of the selected metals, and uncertainties exist based on alloy manufacturing and aging effects. The focus of this report is to provide the measurement uncertainty of the DAS and not the uncertainty of the sensor design.

The remaining measurement uncertainty lies with the capability of the DAS to measure the voltage at the DVM. The thermocouple temperature measurement model flowchart is shown in figure 29. The inputs to the temperature model are the TC junction voltage output, G_{prog}, for the DAS and the change in the ambient temperature. The thermocouple measurement flow chart includes the DVM model.

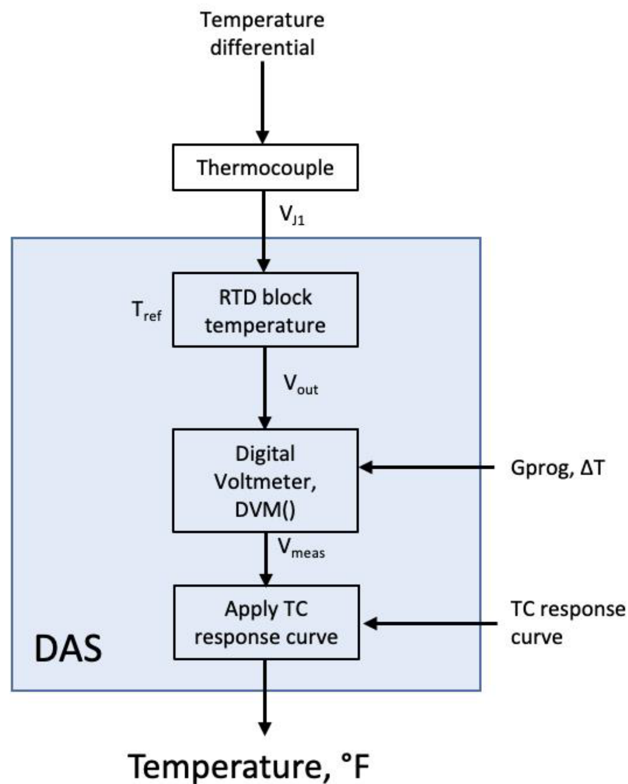

Figure 29. Thermocouple measurement model flowchart.

When measuring Type-K thermocouples, a typical gain setting of 200 is used in the FLL. Setting the gain to 200 millivolt limits the voltage measurement range to ±50 millivolt. The DVM modeling introduced in section 3.2 is used to estimate the uncertainty of the voltage measurement of a Type-K thermocouple ranging from 0 to 50 millivolt, with a gain of 200 millivolt, and an approximate range of 2,250 Fahrenheit degrees. The effect of temperature on the digital voltmeter reading is negligible; therefore, the highest change in lab temperature is provided in the thermocouple measurement uncertainty. The Monte Carlo simulation results for the voltage measurement uncertainty of the DVM (in millivolt) is shown in figure 30.

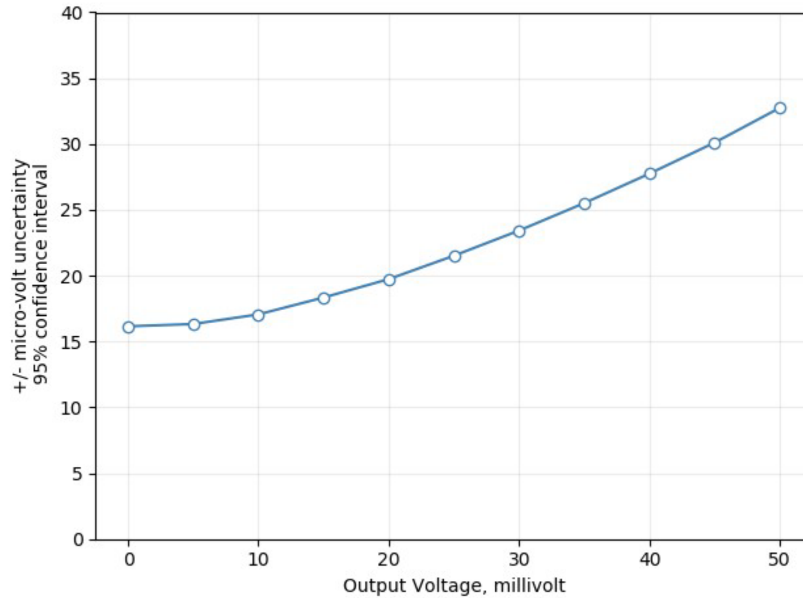

Figure 30. Thermocouple voltage (millivolt), two standard deviations Monte Carlo simulation results.

When the results of the DVM measurement uncertainty is applied to a Type-K thermocouple sensor, the TC temperature measurement uncertainty (in Fahrenheit) is shown in figure 31. Also, evident in figure 31 is the Type-K thermocouple response curve being slightly nonlinear. This nonlinear response is because the temperature-versus-voltage relationship of a thermocouple is nonlinear, and the slope of the curve (i.e., the Seebeck coefficient) is a function of temperature; therefore, the uncertainty in measurement as a function of temperature also exhibits nonlinearities, as shown in figure 31. Reference 7 contains further details on the voltage-to-temperature conversion of thermocouples.

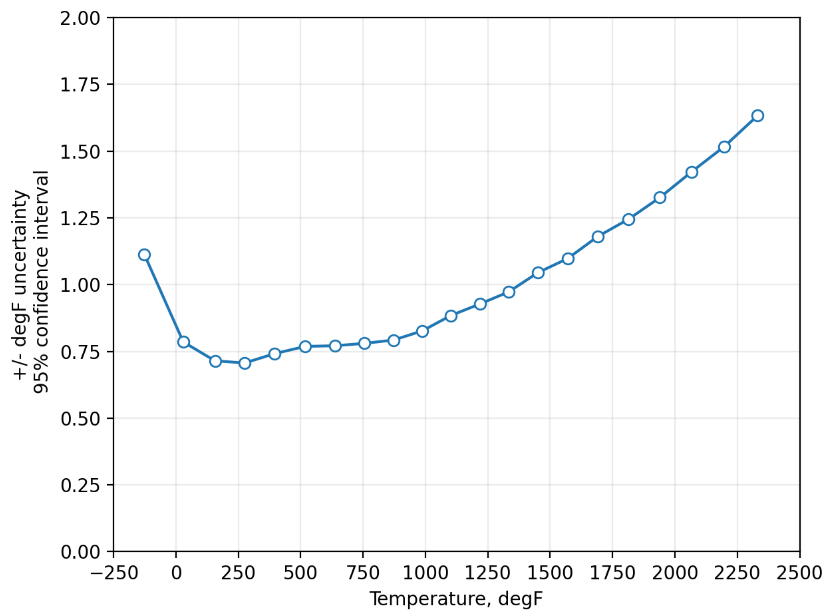

Figure 31. Thermocouple (Type-K) temperature, two standard deviations Monte Carlo uncertainty.

7 Voltage Divider Circuit Monte Carlo Simulation Results

A potentiometer is an adjustable voltage divider device with three electrical terminals. Two fixed terminals are connected to an excitation voltage and are electrically connected by a resistive element. A Third terminal with a sliding contact wiper moves along the resistive element. A voltage divider is produced when measuring the voltage between the terminals connected to the negative terminal of the input voltage and the sliding contact wiper. The sliding contact wiper is then connected with a mechanism that moves the wiper relative to a physical action.

A string potentiometer is a device that converts displacement of a cable to a proportional voltage output. An example of a potentiometer circuit is shown in figure 32. The equation relating slide position as a percentage (SlidePos) to output voltage (V_{out}) is shown is shown in equation 14.

$$V_{out} = V_{in} \times \text{SlidePos} \tag{14}$$

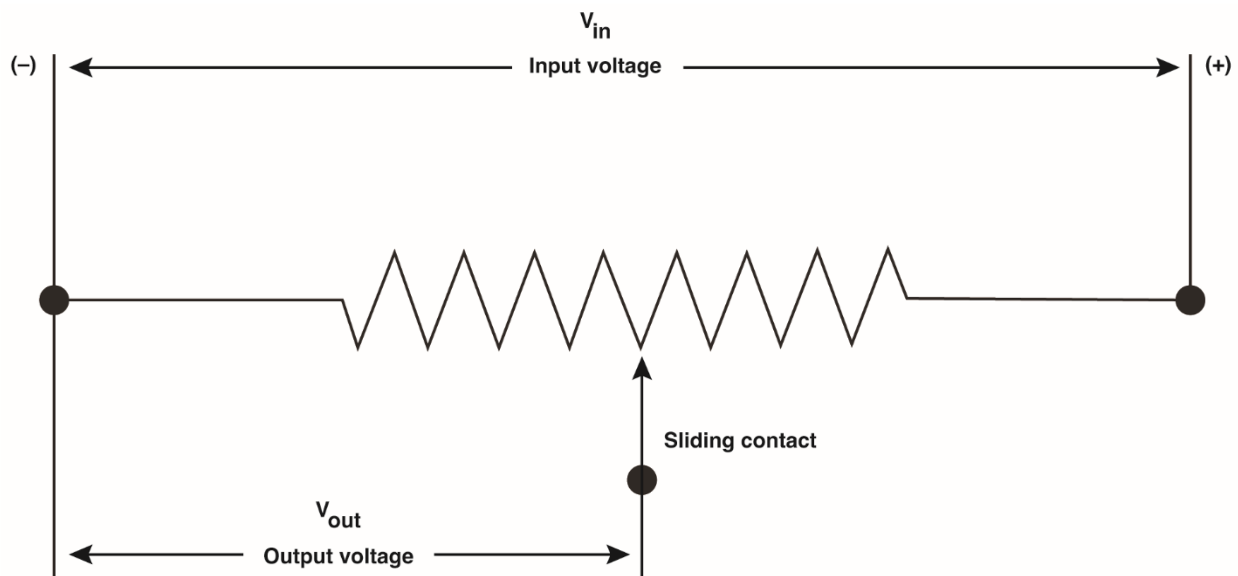

Figure 32. Voltage divider circuit.

The string potentiometer measurement model flowchart is shown in figure 33. Inputs to the string potentiometer model include the input Voltage (V_{in}), Gprog, the string potentiometer sensitivity, and the change in the ambient temperature. The string potentiometer measurement flow chart includes the voltage excitation source model (V_{source}) and the digital voltmeter (DVM) model.

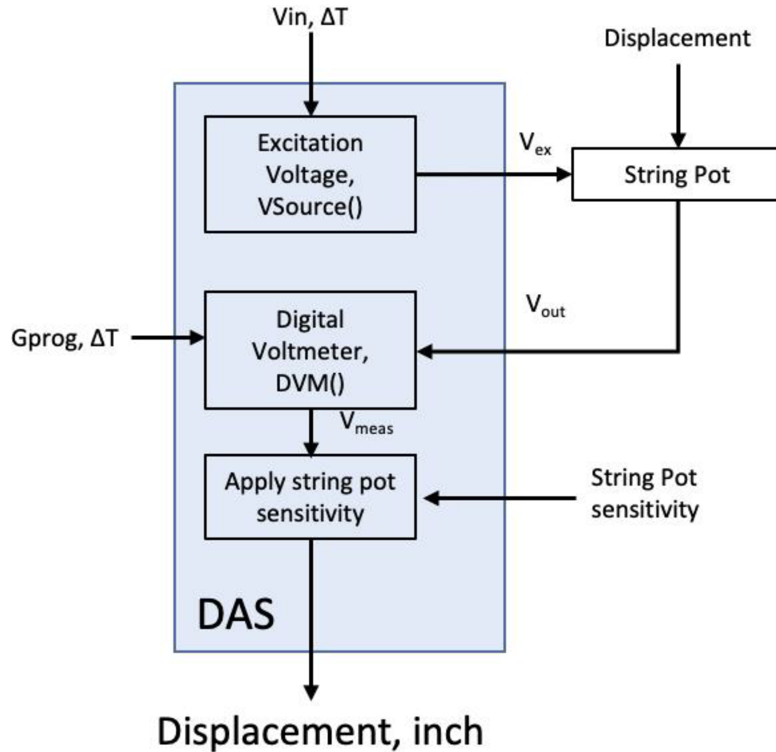

Figure 33. String potentiometer model flowchart.

A Monte Carlo simulation has been performed using an excitation voltage of 10 volt (modeled using the process outlined in section 3.1) and a DVM with gain = 1 (modeled using the process outlined in section 3.2). Typically, displacement of the string potentiometer relative to an initial starting point is a concern among test engineers. Displacements are related to a change in measured voltage between two measurement times. The two separate measurement times are modeled by two different excitation voltages, and the corresponding output voltage is passed through the DVM function. For this simulation, the reference location is set to a slide position corresponding to 50 percent. This setting enables the string potentiometer to experience equal contraction and expansion ranges with a corresponding output voltage change of ±5 volt and a range of 10 volt. The potentiometer position was varied from SlidePos = 0 to 100 percent. The result of the Monte Carlo simulation is shown in figure 34. The effect of temperature on the digital voltmeter reading is negligible; therefore, the highest change in lab temperature is provided in the voltage divider measurement uncertainty, shown in figure 34.

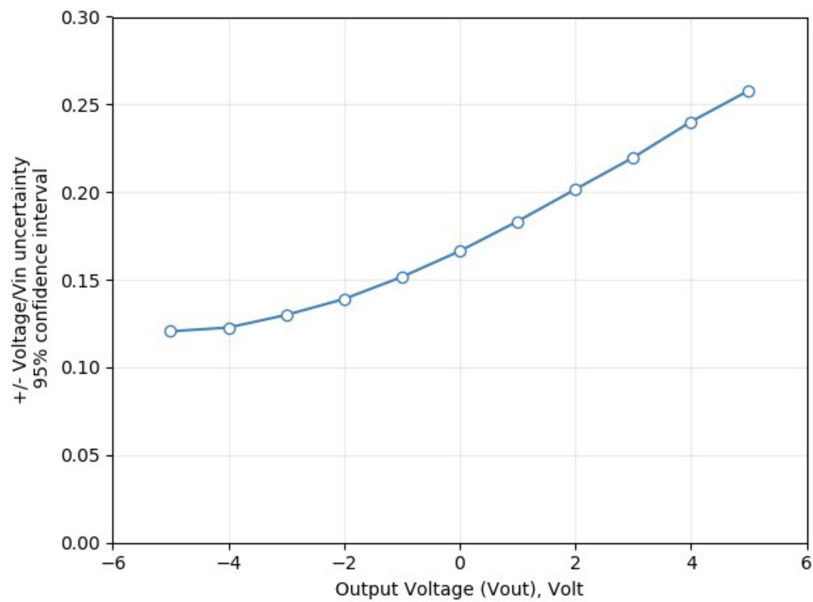

Figure 34. Measured voltage per excitation voltage, two standard deviations Monte Carlo simulation results, V_{in} = 10 V, G_{prog} = 1.

The results shown in figure 34 can be used to estimate the measurement uncertainty for string potentiometers as long as the sensitivity settings are incorporated. In figure 34, the bounded uncertainty of measured voltage per supplied voltage is 0.26 V/V_{in}. The measured voltage per supplied voltage can be scaled by the string potentiometer sensitivity to get an estimate of the measurement uncertainty of displacement.

Various string potentiometer sensing lengths are available commercially. Typical lengths used in the NASA AFRC FLL include 12, 24, 48, 72, and 120 inches. A string potentiometer is selected based on the anticipated displacement range of interest.

As an example, assuming a 120-inch string potentiometer is selected, a typical sensor sensitivity would be approximately 1.2 in/V/V_{in}. The anticipated measurement uncertainty for the 120-inch string potentiometer is shown in figure 35. The estimated uncertainty for a 120-inch string potentiometer would be 0.31 inches (0.26 V/V_{in} × 1.2 in/V/V_{in} = 0.312 in). An example of the typical displacement uncertainties for various string potentiometers is shown in table 6.

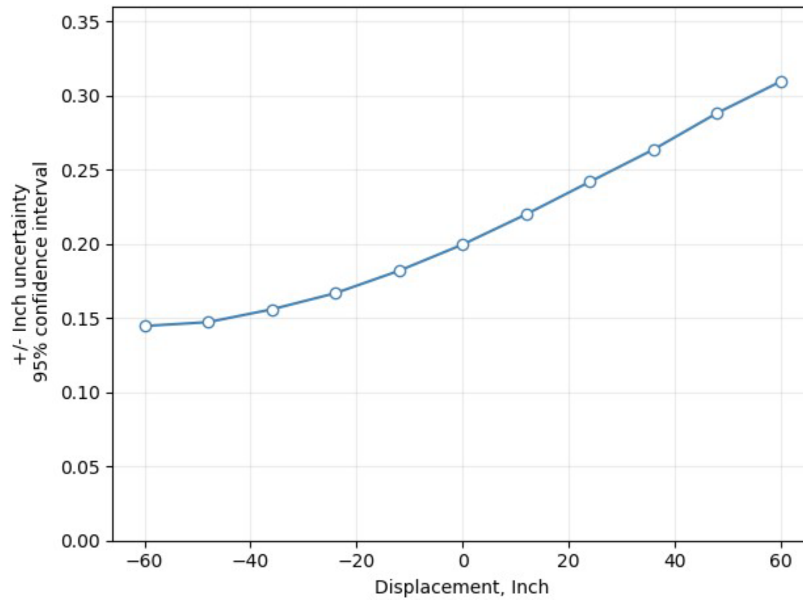

Figure 35. A 120-inch string potentiometer, two standard deviations Monte Carlo measurement uncertainty, sensitivity = 1.2 in/V/V_{in}, V_{in} = 10 V, G_{prog} = 1.

Table 6. Bounded measurement uncertainty for various string potentiometer lengths.

String pot length	V_{in}	G_{prog}	Example string pot sensitivity	Two standard deviations measurement uncertainty
12.0	10.0 V	1.0	0.12 in/V/V_{in}	±0.0312 in
24.0	10.0 V	1.0	0.24 in/V/V_{in}	±0.0624 in
48.0	10.0 V	1.0	0.48 in/V/V_{in}	±0.1248 in
72.0	10.0 V	1.0	0.72 in/V/V_{in}	±0.1872 in
120.0	10.0 V	1.0	1.2 in/V/V_{in}	±0.312 in

The example Monte Carlo simulation results, shown in figure 35, are based on the DAS uncertainty in measuring voltage. There are additional sensor-based measurement uncertainties. The resistive element contained within could have some variability in resistance along its length. A string potentiometer data sheet should also specify the additional error, based on the sensor design. The resistive element within a string potentiometer would be sensitive to changes in temperature. Also, the cable line expands and contracts relative to temperature changes (resulting from thermal expansion) without moving the wiper mechanism. These errors would be sensor-specific based on manufacturing. Additional test setup-specific errors can arise from varying alignment of the cable direction because of test article displacements occurring in more than one axis.

8 Direct Voltage Measurement Monte Carlo Simulation Results

There are some sensors that are either self-powered or have in-line converters and/or digital processors that disassociate the input voltage with the output voltage. Self-powered sensors include, but not limited to, piezoelectric sensors and thermocouples. Some accelerometers used in the FLL are piezoelectric-based sensors. A linear variable differential transformer (LVDT), frequently used in the FLL, is an example of a sensor with an inline converter., which disassociates input voltage and output voltage.

A LVDT is an electrical transformer/sensor that converts linear displacement into an alternating current signal with phase and amplitude content, as shown in figure 36. The LVDT consists of three electrical coils that are aligned along a common axis. A cylindrical-ferromagnetic core, attached to a shaft, moves along a hollow central axis whose displacement is monitored. The central coil is the primary coil that is energized by external power with alternating current; the two remaining coils are called secondary coils. An alternating current drives the primary coil and causes voltage to be induced in each secondary coil by an amount proportional to displacement of the ferromagnetic core. The output signal of an LVDT is an alternating current signal.

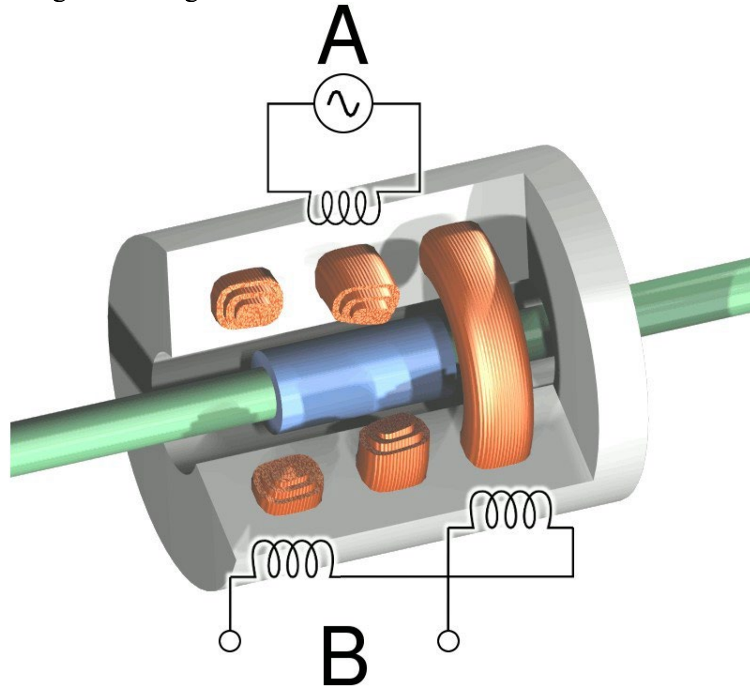

Figure 36. Cutaway view of a linear variable differential transformer.

A signal conditioning device is placed between the original LVDT signal and the DAS. The signal conditioning device contains a demodulator which converts the alternating current voltage signal to a direct current voltage that is proportional to displacement. The direct current voltage output of the demodulator is passed to the DAS. The LVDT measurement model flowchart is provided in figure 37. Inputs to the LVDT model include V_{in}, G_{prog}, the LVDT sensitivity, and the change in the ambient temperature. The LVDT measurement flow chart includes the digital voltmeter DVM( ) model.

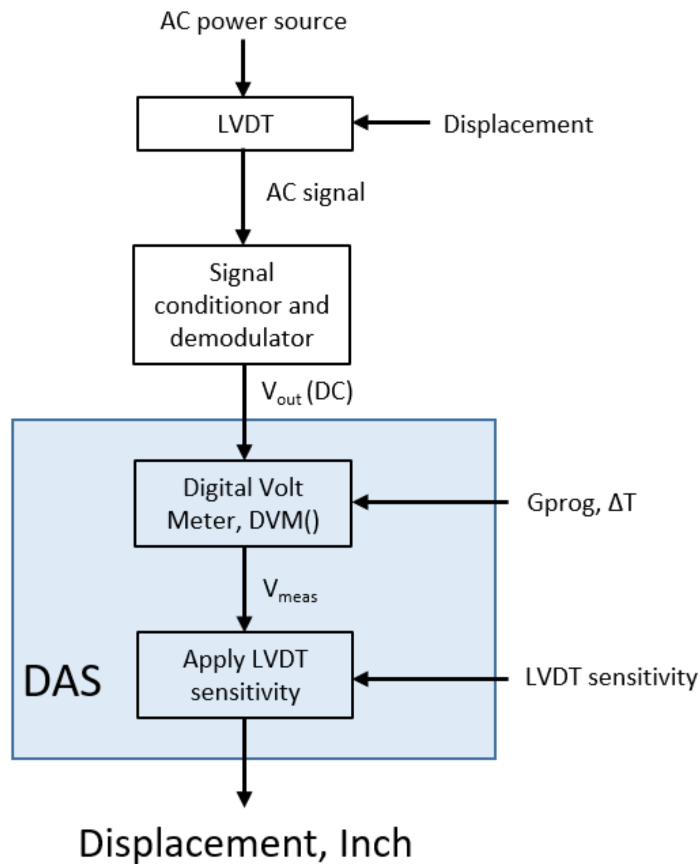

Figure 37. Linear variable differential transformer model flowchart.

For any direct voltage measurement, the output voltage (V_{out}) is sent to the DVM( ) function, as outlined in section 3.2, to obtain the indicated voltage (V_{meas}). A Monte Carlo simulation with 50,000 iterations, and a DVM gain (G_{prog}) set to 1.0 has been processed. The results of the Monte Carlo simulation are shown in figure 38. The estimated bounded uncertainty for a ±10-volt measurement range is ±6.4 millivolt. The LVDT signal conditioning system used in the FLL has a DC output range of ±2.5 volt. The estimated uncertainty for a range of ±2.5-volt measurement is ±3.2 millivolt.

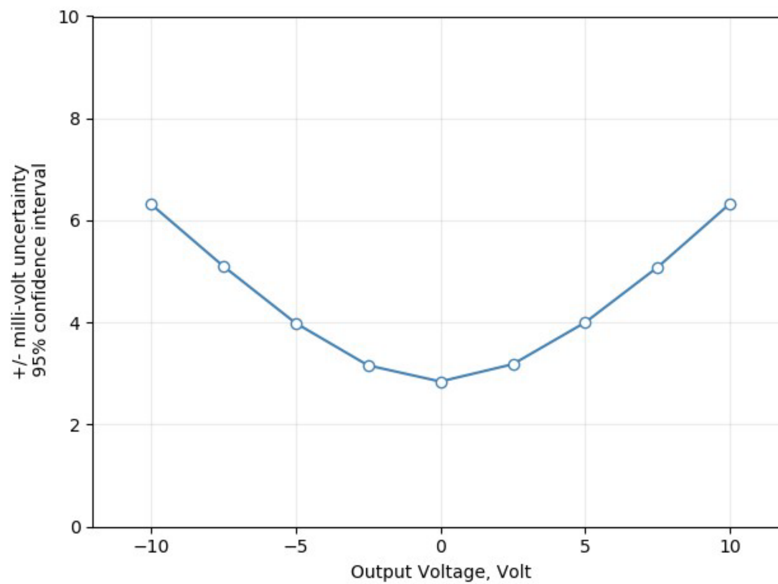

Figure 38. Direct voltage measurement, two standard deviations Monte Carlo results, G_{prog} = 1.

As an example, assuming an LVDT range of ±0.50 inches is selected, and the LVDT signal conditioning system has a direct current voltage range of ±2.5volt, the approximate sensor sensitivity would be approximately 0.2 in/V. The bounded measurement uncertainty over a ±2.5-volt range is ±3.2 millivolt, The anticipated measurement uncertainty for the ±0.50-inch LVDT is provided in figure 39. The estimated uncertainty for a ±0.50-inch LVDT would be 0.64 thousandth of an inch (3.2 mV × 0.2 in/V = 0.00064 in). It is also noted that the LVDT sensitivity definition, presented in this report, may differ from the sensitivity found in the LVDT specification sheet because there is an in-line signal conditioner in the system. An example of typical LVDT bounded uncertainties for various LVDT lengths is shown in table 7.

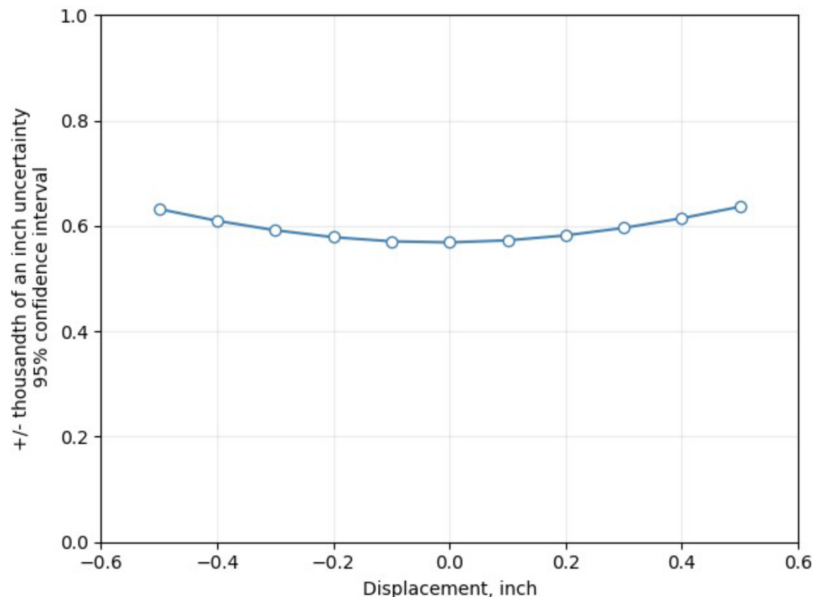

Figure 39. A 0.5-inch linear variable differential transformer, two standard deviations Monte Carlo measurement uncertainty, gain = 1, sensitivity = 0.2 in/V.

Table 7. Bounded measurement uncertainty for various linear variable differential transformer lengths.

LVDT length	G_{prog}	Example LVDT sensitivity	Two standard deviations measurement uncertainty
±0.02 in	1	0.008 in/V	0.0000256 in
±0.05 in	1	0.02 in/V	0.000064 in
±0.1 in	1	0.04 in/V	0.000128 in
±0.5 in	1	0.2 in/V	0.00064 in
±1.0 in	1	0.4 in/V	0.00128 in

The example Monte Carlo simulation results, provided in figure 30, are based on the DAS uncertainty in measuring voltage. Because there are additional sensor-based measurement uncertainties, sensor output may be affected. In the case of the LVDT, there are signal conditioners in the system that may have alternating currents to direct current linearity errors. There are also LVDT linearity errors that contribute to the measurement. These errors would be sensor-specific, based on manufacturing. Additional test setup-specific errors can arise from varying alignment of the sensor relative to the test article.

9 Summary

Throughout this report, measurement uncertainties have been presented for various analog sensor types that are used in the National Aeronautics and Space Administration Armstrong Flight Research Center Flight Loads Lab. These measurement uncertainties were determined by developing models of representative data acquisition system components used in the Flight Loads Lab and incorporating these uncertainties using a random number generator with a normal distribution. These data acquisition system models were then included in each sensor circuit model. Each sensor circuit model was then analyzed using the Monte Carlo method to obtain an estimate of the two standard deviations of measurement uncertainty. These common sensors include the following: foil strain gages, load cells, thermocouples, voltage divider circuits, and direct voltage measurements. Several strain-gage circuits have been presented including the Quarter-bridge; Half-bridge (Type-I and Type-II); and Full-bridge (Type-I, Type-II, and Type-III).

The representative range for all strain-gage types used in the Flight Loads Lab was ±3,000 microstrain. The temperature ranges during testing in the Flight Loads Lab were estimated to stay below ±4 Fahrenheit degrees. A summary of the typical measurement uncertainties for analog sensors used in the Flight Loads Lab are presented within the report. The process that was used and presented in this report can be adapted to represent any other data acquisition module, as long as documentation regarding performance is provided.

Table 8. Summary of typical measurement uncertainties for various analog sensors.

Measurement type	V_{in}	Gain	Range	Ambient temperature change	Two standard deviations measurement uncertainty
Strain: Quarter-bridge	5.0	300	±3,000 με	±4 °F	±13 με
Strain: Half-bridge, Type-I	5.0	300	±3,000 με	±4 °F	±10 με
Strain: Half-bridge, Type-II	5.0	300	±3,000 με	±4 °F	±8 με
Strain: Full-bridge, Type-I	5.0	150	±3,000 με	±4 °F	±8 με
Strain: Full-bridge, Type-II	5.0	150	±3,000 με	±4 °F	±8 με
Strain: Full-bridge, Type-III	5.0	150	±3,000 με	±4 °F	±8 με
Load cell (voltage)	10.0	200	±3 mV	±4 °F	±7.2 $\mu V/V_{in}$ × sensitivity
Thermocouple, Type-K	N/A	200	72 to 2,000 °F	±4 °F	±1.7 °F
Voltage divider (string pot)	10.0	1	0 to 10 V	±4 °F	0.26 V/V_{in} × sensitivity
Direct voltage (LVDT)	N/A	1	±2.5 V	±4 °F	±3.2 mV × sensitivity*

* The linear variable differential transformer (LVDT) sensitivity is defined in this report and is based on the LVDT displacement range divided by signal conditioner voltage range. This sensitivity definition may differ from a vendor supplied LVDT specification sheet.

10 References

1. Coleman, Hugh W., and W. Glenn Steele, *Experimentation, Validation, and Uncertainty Analysis for Engineers*, 3rd Ed., Hoboken, New Jersey, John Wiley & Sons, Inc., IBN: 978-0-470-16888-2, 2009.
2. National Institute of Standards and Technology (NIST), "Measurement Uncertainty," created September 29, 2010, updated June 2, 2021. https://www.nist.gov/itl/sed/topic-areas/measurement-uncertainty Accessed April 15, 2025.
3. International Bureau of Weights and Measures (BIPM), *Joint Committee for Guides in Metrology (JCGM), Evaluation of measurement data — Supplement 1 to the "Guide to the Expression of Uncertainty in Measurement" — Propagation of distributions using a Monte Carlo method*, first edition 2008, JCGM 101.2008. https://www.bipm.org/utils/common/documents/jcgm/JCGM_101_2008_E.pdf Accessed April 15, 2025.
4. Vishay Micro-Measurements, *Model P3 Strain Indicator and Recorder, Instruction Manual*, Vishay Micro-Measurements, Raleigh, North Carolina, 130-000109, March 2005.
5. Hewlett-Packard Co., Application Note 290-1: *Practical Strain Gage Measurements*, Hewlett-Packard Co., Palo Alto, California, September 1981.
6. Vishay Micro-Measurements, *Shunt Calibration of Strain Gage Instrumentation*, Tech Note TN-514. Vishay Micro-Measurements, Raleigh, North Carolina, February 2013.
7. Hewlett-Packard Co., Application Note 290: *Practical Temperature Measurement*s, 5952-8801, Hewlett-Packard Co., Palo Alto, California, 1983.
8. National Institute of Standards and Technology (NIST), "NIST: ITS-90 Table for type K thermocouple," https://srdata.nist.gov/its90/download/type_k.tab. Accessed April 15, 2025.